

UC San Diego

UC San Diego Electronic Theses and Dissertations

Title

Getting a grip underwater: The suction disc of the northern clingfish inspires a reversible underwater adhesion mechanism

Permalink

<https://escholarship.org/uc/item/77c500qh>

Author

Sandoval, Jessica ALEXANDRA

Publication Date

2018

Peer reviewed|Thesis/dissertation

UNIVERSITY OF CALIFORNIA, SAN DIEGO

Getting a grip underwater: The suction disc of the northern clingfish inspires a reversible
underwater adhesion mechanism

A Thesis submitted in partial satisfaction of the requirements
for the degree Master of Science

in

Mechanical and Aerospace Engineering

by

Jessica Alexandra Sandoval

Committee in charge:

Michael T. Tolley, Chair

Dimitri D. Deheyn

Marc A. Meyers

2018

Copyright

Jessica Alexandra Sandoval, 2018

All rights reserved.

The Thesis of Jessica Alexandra Sandoval is approved, and it is acceptable in quality and form for publication on microfilm and electronically:

Chair

University of California, San Diego

2018

DEDICATION

For all of her support, guidance, and boundless love, I dedicate this thesis to my mom.

TABLE OF CONTENTS

Signature Page	iii
Dedication	iv
Table of Contents	v
List of Figures	viii
List of Tables	xii
Acknowledgements	xiii
Abstract of the thesis	xiv
Chapter 1: Introduction	1
1.1 Mechanisms for adhesion in biological systems.....	1
1.2 Current applications of underwater grip	6
1.3 Overview of research presented in thesis	7
Chapter 2: The hierarchical mechanisms of adhesion of the suction disc of the northern clingfish	9
2.1 Experimental Set-Ups	12
2.1.1 Sample collection and preparation	12
2.1.2 Imaging techniques.....	12
2.1.3 Pull-tests.....	13
2.2 The structures of adhesion of the clingfish.....	19

2.2.1 The role of the suction chamber.....	14
2.2.2 Characterization of the pads	19
2.2.3 The role of the fibrils	24
2.2.4 Capillary adhesion estimation with scaled pull-tests.....	27
2.3 Conclusion	33
Chapter 3: A biomimetic suction disc: Design and performance of clingfish-inspired adhesive technology	35
3.1 Mechanisms to mimic	35
3.2 Fabrication of the artificial suction discs.....	38
3.3 Evaluation of suction disc performance	41
3.3.1 Maximum normal stress measurements: Experimental Setup.....	41
3.3.2 Frustrated Total Internal Reflection of the disc foot print: Experimental setup.....	43
3.3.3 Results and Discussion	44
3.4 Conclusion and Future Work	54
Chapter 4: Application of the biomimetic suction disc: Underwater Robotics and Sensing.	56
4.1 Archaeological Applications	56
4.1.1 First iteration of a passive gripper	57
4.2 Design of a sensor package	59

4.3 Application of suction discs to underwater locomotion	60
4.4 Future applications of the artificial suction disc	60
Conclusion	61
Bibliography	63

LIST OF FIGURES

- Figure 1.1: Suction discs across body sizes of clingfish. A** *Sicyases sanguineus*. **B** *Tomicodon humeralis*. **C** *Gobiesox*. **D** *Gobiesox*. **E** Posterior disc margin. Preserved specimen from Marine Vertebrate Collection at Scripps Institution of Oceanography..... 5
- Figure 2.1: The mechanism of adhesion of the clingfish is hierarchical. A** A clingfish adheres onto a glass slide post mortem. **B** The suction disc of the clingfish consists of an empty chamber “EC” surrounded by a perimeter of soft pads. **C** A representation of the structures involved in adhesion of the clingfish. Ventral view. **D** Lateral view of the clingfish..... 10
- Figure 2.2: Overview of the biological mechanism of adhesion in the clingfish, corresponding to Table 2.1. A** Suction chamber, for bonding via suction. **B** Pad, for capillary adhesion. **C** Fibrils, for friction and micro-scale interlocking.....11
- Figure 2.3: Force balance of clingfish suction chamber.** The detachment force, F_d , is equal to the force created by atmospheric pressure, P_{atm} . Force due to buoyancy, F_b . Force due to gravity, F_g . Friction (F_f) is lateral force opposing slip (F_{slip})..... 14
- Figure 2.4: Left Averaged pull-off force of euthanized clingfish, demonstrated directional adhesion.** Clingfish pulled forward 2 cm prior to removal from surface, 3 trials (blue). Clingfish pulled backwards 2 cm prior to removal from surface, 4 trials (red). Clingfish removed from surface without directional pull, 3 trials (green). Rate of removal, 8 mm/s..... 15
- Figure 2.5: Ventral views of the orientations of a live clingfish during adhesion, imaged under Frustrated Total Internal Reflectance. A** Disc and head in contact with imaging surface. Two suction chambers created. **B** Anterior disc margin and head in contact creating one cavity. **C** Only suction disc engaged with imaging surface. One cavity formed..... 16
- Figure 2.6: Time series of a disassociation event. A** The intersection of the pelvic and pectoral fins was gently prodded with a rounded probe, outlined in red. **B** The pressure of the chamber increases to ambient pressures. **C-D** Progressive disassociation of clingfish disc margin..... 18
- Figure 2.7: Eccentricity of an ellipse. a:** semi-major axis length. **b:** semi-minor axis length. **c:** distance from the center to foci, **f**..... 19
- Figure 2.8: An overview of the image processing procedures to generate a high-resolution map of the pads of the disc margin. Left to Right** High magnification images were stacked and stitched together using a custom-built algorithm. The resulting map, presented as a black and white figure, was then run through a region processing algorithm..... 20
- Figure 2.9: Scanning Electron Micrographs of pad on disc margin reveal extensive microchannel network. A** Single pad on the disc margin. **B** The entirety of the surface of the pad is an elaborate system of microchannels with an average diameter of 0.25 μm . **C** A fracture along the edge of the pad reveals soft fibrillar extrusions 21
- Figure 2.10: Transmission Electron Micrograph of a pad. A** A semi-thin tissue section was prepared. Three distinct layers of tissue are distinguishable. Orientation of cuts indicated by the

clingfish schematic in the lower left-hand corner. **B** Microchannels are expressed on the surface of the pad. Average diameter of channel 0.25 μm at a spacing of 0.02 μm 23

Figure 2.11: Atomic Force Microscopy to determine adhesive strength of fibrils and secretions. **A** View of probe tip over pad. **B** Setup of AFM measurement occurred in droplet of filtered sea water as to hydrate the sample. **C** Example force curve with two unbinding events..25

Figure 2.12 Average force (nN) of adhesion for regions of the clingfish pad. **A** The upper pad refers to the anterior disc margin, which had the largest force of adhesion. **B** Finned regions refers to the pads on a fin of the disc margin. **C** Secretions were isolated and vortexed prior to interrogation by AFM..... 25

Figure 2.13: Secretions present on dried clingfish footprint. **A** View of clingfish footprint on a glass slide, imaged under Brightfield microscopy. **B** Glycoprotein ferning patterns evident along suction disc margin. **C** Geometric shape and orientation of secretions..... 27

Figure 2.14: Stefan Adhesion acting between two parallel plates when separated. Plates of radius R , fluid of viscosity η 28

Figure 2.15: Scaled adhesion experiment to test contribution of Stefan adhesion to total adhesive capabilities of the clingfish. **A** Pad array in contact with flat surface in a bath of glycerol. **B** Array of pads pulled perpendicular from surface and the adhesive stress was calculated..... 29

Figure 2.16: Geometries of scaled array of pads for tests of Stefan adhesion. Computer renderings of scaled pads with three stiffness, pink being the most compliant and dark red being the least. Based on analysis of TEM micrographs (center)..... 30

Figure 2.17: Fillets affect adhesive force of scaled pads and is rate dependent. Non-filleted pads, blue square. Filleted pads, red circle. Speed of Retraction: Slow (0.001 mm/s), Moderate (0.01 mm/s), Fast (0.1 mm/s). Note the difference in y-axis scale..... 31

Figure 2.18: Example raw data adhesive force curves: Fillets with two disassociation events. **Left** Non-filleted pads. **Right** Filleted pads. Speed of Retraction: Moderate (0.01 mm/s). In both figures, pads were preloaded to 10N..... 32

Figure 3.1: Clingfish suction disc inspires structure and material properties of an artificial suction disc. **Left** Overview of the hierarchy of adhesion of the clingfish suction disc. **A** Intricate muscle network for dynamic control of suction disc. **B** Secretions for sealing internal low pressure chamber..... 36

Figure 3.2: Geometries of suction disc low-pressure chambers. **Left** Clingfish body cavity geometry. **Right** Circular body cavity with four slits. All units in millimeters..... 38

Figure 3.3: Fabrication of low pressure chamber. **A** Computer Aided Design (CAD) model of the mold of the suction disc. **B** Mold 3D printed on the Stratasys Objet350 Connex3. Suction disc (left) molded with DragonSkin 20..... 39

Figure 3.4: Prototype variations. Left are computer renderings of the prototype. Green circles indicate that the feature is present in the prototype. Soft layer is a 2 mm layer of Ecoflex 00-30. Slits are cuts made in the disc margin. Symmetry was either radial (circular) or bilateral (mimic of fish geometry)..... 40

Figure 3.5: Setup of adhesive stress tests performed on the Instron 3342. The substrate was submerged in a body of water. Unloading at constant rate. The load cell, L, records the force and extension, which can be used to calculate force and time curves..... 42

Figure 3.6: Setup of surfaces on which pull tests were conducted. Surface roughness experiments were tested on flat plates. Concavity experiments were tested on halved PVC pipes. The combination of the effects of concavity and texture was evaluated on PVC with sand paper adhered to the surface..... 43

Figure 3.7: A An artificial suction disc picks up a cratered stone. **B** An artificial suction disc picks up the concave surface of a fractured granite rock. **C** An artificial suction disc lifts a 625 gram granite rock. All tests were performed and imaged underwater..... 44

Figure 3.8: Layer of Ecoflex needed for adhesion on rough surfaces, findings of the flat plate pull tests on variable surface roughnesses. Comparison of performance of five prototypes against a commercially available suction cup. Pull test performed in bath of water, three pull tests per disc..... 45

Figure 3.9: Pull-tests on smooth convex surfaces. The commercial suction cup (red triangle) had highest pull-off forces on smooth convex surfaces. Pull test performed in bath of water, three pull tests per disc..... 47

Figure 3.10: Pull-tests on smooth concave surfaces. The artificial disc with a soft layer and four slits had highest adhesive stress at the smallest diameter of a concave surface. Pull-test performed in bath of water, three pull-tests per disc..... 48

Figure 3.11: Pull-tests on rough concave surface. The discs and commercial suction cups were tested on a concave surface of 41 mm diameter and a roughness of 269 μm . Pull test performed in bath of water, three pull tests per disc..... 49

Figure 3.12: Frustrated Total Internal Reflection (FTIR) to visualize the footprint of selected prototypes. The discs were placed on the imaging plate (“Rest”), depressed to the surface (“Push”), and pulled from the surface (“Pull”)..... 50

Figure 3.13: Slits are critical to conforming to non-planar shapes of a substrate. Left Irregular shapes compromise the low-pressure chamber of suction discs without slits. The disc margin “leaks” when not slitted. **Right** Slits allow the disc margin to expand and cover irregularities in shape and texture, thus maintaining the seal to the low-pressure chamber..... 52

Figure 3.14: A suction disc adheres to a river stone to which a payload is secured and increases in weight overtime. Payload (rice dyed blue for visualization). Performed in air... 53

Figure 4.1: Suction disc adhering to and lifting an example of an archaeological artifact while underwater...... 57

Figure 4.2: The first iteration of the passive gripper was designed for archaeological applications. However, the first iteration was unsuccessful at equally distributing the load across many suction discs..... 58

Figure 4.3: Camera mount using an artificial disc to adhere to rough surfaces underwater..... 59

LIST OF TABLES

Table 2.1: Scales and mechanisms of adhesion in clingfish..... 11
Table 2.2: Averaged adhesive force of scaled pads versus speed of retraction..... 31

ACKNOWLEDGEMENTS

I would like to thank Dr. Michael T. Tolley, Dr. Dimitri D. Deheyn, and Dr. Marc A. Meyers for their support and encouragement over the course of my thesis. I would like to acknowledge the Scripps Marine Vertebrate Collection for the generous use of their archived clingfish specimen. I would like to thank Haocheng Quan for his help and experimental expertise. I would like to acknowledge Nirav Patel for his guidance on Atomic Force Microscopy. And to Alexa Zonderman for her assistance in field and lab experiments.

I would like to thank the many incredible researchers and scholars I have met and collaborated with along the way, including the BRDL Turtles.

Chapter 2, in part is currently being prepared for submission for publication of the material. Sandoval, Jessica; Quan, Haocheng; Meyers, Marc A.; Tolley, Michael T.; Deheyn, Dimitri D. "The hierarchical mechanisms of adhesion of the suction disc of the northern clingfish". The thesis author was the primary investigator and author of this material.

Chapter 3, in part is currently being prepared for submission for publication of the material. Sandoval, Jessica; Quan, Haocheng; Deheyn, Dimitri D.; Tolley, Michael T. "A biomimetic suction disc: Design and performance of clingfish-inspired adhesive technology on irregular surfaces". The thesis author was the primary investigator and author of this material.

Chapter 4, in part is currently being prepared for submission for publication of the material. Sandoval, Jessica; Quan, Haocheng; Deheyn, Dimitri D.; Tolley, Michael T. "A biomimetic suction disc: Design and performance of clingfish-inspired adhesive technology on irregular surfaces". The thesis author was the primary investigator and author of this material.

ABSTRACT OF THE THESIS

Getting a grip underwater: The suction disc of the northern clingfish inspires a reversible underwater adhesion mechanism

by

Jessica Alexandra Sandoval

Master of Science in Mechanical and Aerospace Engineering

University of California, San Diego, 2018

Professor Michael T. Tolley, Chair

Non-destructive reversible adhesion is difficult to achieve on rough surfaces underwater. In an effort to design a mechanism of reversible adhesion, we sought inspiration from the northern clingfish (*Gobiesox*), which has evolved the impressive ability to stick onto irregular substrates while subject to intertidal surges. The mechanisms of adhesion in the biological system were investigated and applied to an engineered mimic. The artificial suction disc adhered to rough surfaces and non-planar shapes, outperforming commercial suction cups

and on par with the performance of the clingfish. This design has many potential applications, including underwater manipulation, sensor packages, and soft robotic locomotion.

Chapter 1

Introduction

Many mechanisms for adhesion in air do not stick underwater. The engineered solutions currently available are limited and none yet match the specifications of being reversible and nondestructive while adhering to rough and non-flat surfaces. Yet an engineered solution that matches these criteria would help transform the fields of underwater manipulation, locomotion, and sensor development. This would affect a range of industries, from ocean exploration to wildlife management.

1.1 Mechanisms for adhesion in biological systems

Adhesion in air can be achieved by several methods, including van der Waals interactions, chemical binding, and suction forces [1]. However, mechanisms for adhesion in air do not all apply underwater. We looked to nature to provide examples of adhesion mechanisms that could be readily mimicked.

Adhesion mechanisms in organisms has been classified into the categories of friction, mechanical interlocking, and bonding [2] [3]. Friction is an interaction on a microscopic scale between an organism and surface irregularities. Mechanical interlocking involves the use of macroscopic structures, such as hooks or claws, to penetrate into a surface to achieve attachment. Bonding is broadly defined as forming a bond with a surface, either through chemical adhesion, dry adhesion (van der Waals), capillarity, or suction. In order to develop a non-destructive reversible adhesion, we avoided systems that rely heavily on chemical bonding, for instance.

van der Waals forces are promising for reversible adhesion in air. From arthropods such as spiders to reptiles such as geckos, evolution has favored the independent development of this adhesion mechanism across species. The foot of the jumping spider for instance is covered in setules, which are hairs with broad, sail-like terminations with an average adhesive force of 41 nN [4]. The orientation of the setules is uniform across the area of the foot, and demonstrates a preference in directionality. Similarly, geckos also have foot pads that are covered in setae with a density of 5300/mm² [5]. The setae are projections that are described as tree-like in their structure. Each seta is branched into hundreds of spatulae roughly 100 nm in size, and contributes roughly 20 μ N to the total adhesive force. Both organisms employ dry adhesion in order to adhere to surfaces.

Dry adhesives inspired by the gecko have been engineered using microfabrication techniques to create adhesives that employ van der Waals forces [6]. These engineered adhesives function optimally in air and have been applied with much success to soft robotic grippers to improve grip [7]. However, the application of engineered dry adhesives in water has been less than successful. Conversely, marine organisms have been shown to employ van der Waals forces for adhesion. For instance, the red abalone has setae on the pedal foot, similar to those of the

gecko [3]. Adhesive forces of each individual setae were measured at 600 nN in an experiment of varying humidity. This demonstrated the combined effect of van der Waals and capillary forces to abalone attachment and adhesion in an aquatic environment.

Mechanical interlocking is another mechanism of adhesion of biological organisms. Mechanical interlocking physically secures the organism to a surface. An example of an organism that employs mechanical interlocking as a mechanism for adhesion is the remora. The remora is a fish commonly physically associated with sharks, whales, and rays, and achieves attachment to its host through a modified dorsal suction disc [8]. In order to withstand highly directional flow along the body of the host organism, the suction disc of the remora mechanically interlocks using rigid spines to secure itself against the body of its host. The spatial frequency of the spines has evolved to be nearly identical to the features of the host organism, such as the denticles of sharks. This allows for a near lock-and-key fit of the spines to the surface, thus maximizing securement. This interlock is coupled with a shallow fleshy suction disc to also create a low-pressure chamber in order to further prevent dislodgement of the remora in high-flow conditions.

A robotic analog has been designed using the structure of the remora as inspiration [9]. This robotic suction disc uses rigid spines to provide an anchor and withstands highly directional flow. The spines are also controlled in order to enlarge the depth of the suction chamber and further enhance the contribution of suction. This robotic analog requires actuation and a combination of rigid and soft components in order to achieve adhesion. We aimed to simplify the design of the suction disc and achieve large strengths of adhesion without the requirement of actuation.

Suction is also a common strategy for underwater adhesion. An example of suction is the sucker of an octopus, which is used for grabbing and manipulating underwater objects. Suckers line the ventral surface of the octopus arm and are generally circular in shape. The suckers are composed of two thick muscles, the infundibulum and the acetabulum, which are controlled via muscle contractions. The control of the two muscles allows for dynamic grip by the octopus arm on underwater substratum. A matrix of many suckers is the key concept for the strong gripping abilities of the octopus, as it has many points of suction [10].

In order to develop a gripping mechanism for use underwater on rough surfaces without necessitating an array of suckers, attention was turned to the modified suction discs of fishes. One striking example is the Pulin river loach, which is known for its climbing ability up waterfalls [2]. The entire body of the loach forms a suction disc, which is lined by setae to seal the edge of the suction disc by interlocking with irregularities on the surface. The lips of the loach are also lined by hexagonal protrusions, unculi, originating from keratinized epithelial cells, which are hypothesized to rigidly interlock with surfaces much like a hook. The loach achieves a pull-off stress of on average 30 kPa across rough and smooth substrate. The body geometry and the hillstream environment of the river loach suggest the fish performs optimally in a directional flow scenario.

The northern clingfish was selected for its ability to adhere to rough substrate and resist normal pull-off forces. The clingfish lives in intertidal environments and adheres to rough, irregular, and biofouled surfaces [11]. Clingfish are a part of the family Gobiesocidae that has proliferated across continents. The functionality of the suction disc remains the unifying factor across body shapes and sizes. For instance, *Sicyases sanguineus* (Figure 1.1A), a clingfish native to Chile, has a suction disc that is an order of magnitude larger than that of *Gobiesox* (Figure 1.1

C), a clingfish collected from the California coastline. The function of the disc therefore translates across body size and geographic location, emphasizing an importance in the adhesive disc design.

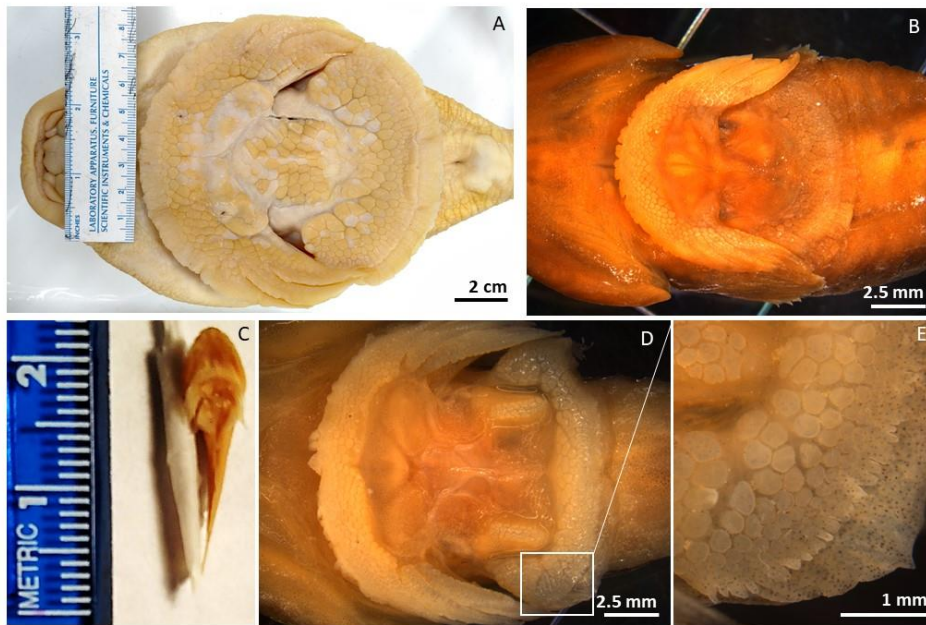


Figure 1.1: Suction discs across body sizes of clingfish. A *Sicyases sanguineus*. **B** *Tomicodon humeralis*. **C** *Gobiesox*. **D** *Gobiesox*. **E** Posterior disc margin. Preserved specimen from Marine Vertebrate Collection at Scripps Institution of Oceanography.

Previous work done on the clingfish (*Gobiesox maeandricus*) demonstrates an impressive adhesive capability of withstanding normal forces that are 80 to 230 times its body weight, the peak stress between 20 and 50 kPa [11]. The clingfish outperformed commercial suction cups on textured surfaces. The structure of the clingfish suction disc is formed by modified pelvic and pectoral fins, and includes two posterolateral vents where the fins converge [12]. Along the perimeter of the suction disc are a thick array of pads that express papillae structures. As proposed in previous literature, the papillae structures have diameters of around 0.2 μm and were

similar to the adhesive setae of spiders and geckos [11]. However, the mechanism of adhesion performed by the papillae had not been explored in previous literature. Thus in order to understand these structures and how to apply them to an artificial mimic, the underlying function of the papillae first needed to be explored.

1.2 Current applications of underwater grip

The applications of non-destructive underwater adhesion extend into the fields of underwater manipulation and sensor platforms. Currently, manipulators that are used in ocean exploration have been repurposed from the oil and gas industry, and thus are built for rigidity, not delicately handling specimens. In order for a robot to grasp underwater objects delicately, it needs a soft touch. The recent innovation of soft robotics seems a promising addition to underwater exploration and manipulation. Soft robotics is a field of robotics that employs the use of compliant materials as an alternative to rigid bodies. The compliant material allows for increased adaptability to its environment and more delicate interaction with objects. Ocean exploration has begun to encompass the field of soft robotics. Manipulators such as the boa-inspired gripper are designed specifically for manipulation and harvesting of deep sea corals [13]. This manipulator, when integrated onto a Remotely Operated Vehicle (ROV), has the capability to gently harvest long, flexible, cylindrical corals and serves as an example of bioinspired soft robotic manipulators tailored for deep sea exploration.

A second example of soft robotic manipulators for ocean exploration is a particle jamming gripper, which is a gripper filled with granular material that is able to conform to an object when a vacuum is applied [14]. This method of particle jamming is most effective in air,

as friction along the gripper is required to maintain grip. This method is not as effective underwater as in air since a fluid film layer forms between the gripper and the object and significantly reduces the contribution of friction to adhesion to the object [15].

The third gripper type is a suction cup, commonly used in archaeological dives and recoveries. A suction cup is an example of a soft adhesion technique and has been used for manipulation of underwater artifacts. A suction cup functions by creating a chamber of lower pressure in comparison to the surrounding fluid. The simplest of the three underwater soft gripping techniques detailed in this section, the suction cup does not require actuation once a pressure differential is established between its inner chamber and the surrounding fluid. However, although suction cups hold well to flat, smooth surfaces, they fail to function on rough surfaces and irregular, non-planar shapes.

1.3 Overview of research presented in thesis

In order to create a non-destructive, reversible mechanism of adhesion that functions with little actuation on rough surfaces, we performed biological investigations into the suction disc of the northern clingfish and applied the mechanisms to design an artificial analog. As detailed in Chapter 2, we first investigated the hierarchical mechanisms of adhesion of the clingfish, which encompass micro- and macroscopic contributions. As detailed in Chapter 3, we then learned from these biological findings in order to apply them to create artificial suction discs. As detailed in Chapter 4, the artificial suction discs were then applied to passive underwater grippers and sensors, as examples of future applications of the technology. It is through this process of learning from nature and applying the designs were we able to create artificial suction discs that

outperform commercially available suction cups on rough and granular textures and non-planar body geometries.

Chapter 2

The hierarchical mechanisms of adhesion of the suction disc of the northern clingfish

The northern clingfish has an impressive ability to adhere to rocky substrate in the intertidal and withstand wave action [16]. This capability made it a model organism for our investigation into reversible adhesion onto variable underwater surfaces. Previous work has included the use of Scanning Electron Microscopy (SEM) to investigate the structures of adhesion of the clingfish. However, in order to gain further understanding, we not only performed SEM but also imaged the sample under Transmission Electron Microscopy (TEM) and tested the adhesive performance of its structures using Atomic Force Microscopy (AFM). With a more complete understanding of the mechanisms of adhesion at play in the biological organism, it became feasible to mimic the concepts in order to create an artificial analog. Thus,

the success of the engineered system is hinged on the biological investigations that were first performed.

The clingfish adheres onto surfaces using suction, where water is displaced from a suction chamber at the intersection of the pelvic and pectoral fins [12]. The displacement of water induces suction by creating a chamber of sub-ambient pressure. A perimeter, referred to in this study as the disc margin, is covered in pads and acts to seal the inner chamber (Figure 2.1 B). This disc margin is critical in the success of the clingfish to hold onto rough surfaces. The disc margin prevents failure in the walls of the suction chamber, which would otherwise be compromised on rough surfaces. The disc margin is further sealed by a layer of non-adhesive secretions (Figure 2.1D).

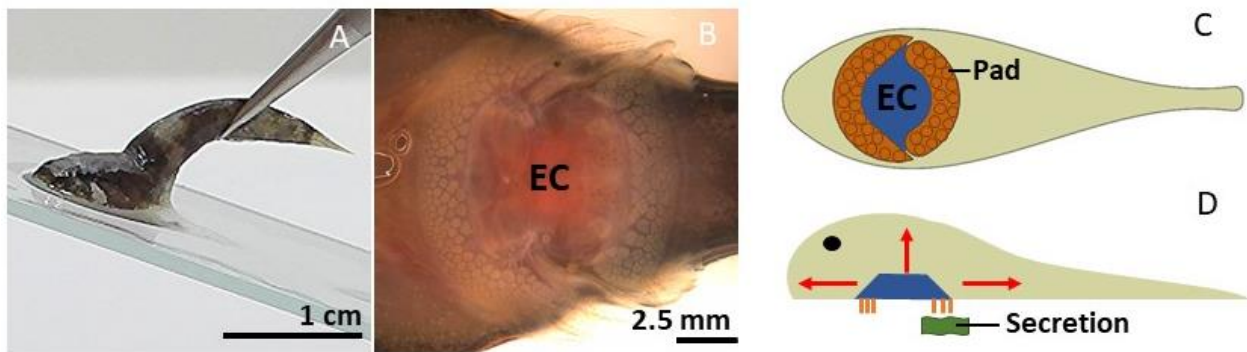


Figure 2.1: The mechanism of adhesion of the clingfish is hierarchical. **A** A clingfish adheres onto a glass slide post mortem. **B** The suction disc of the clingfish consists of an empty chamber “EC” surrounded by a perimeter of soft pads. **C** A representation of the structures involved in adhesion of the clingfish. Ventral view. **D** Lateral view of the clingfish. The blue trapezoid is the concavity of the suction chamber.

As discussed in Chapter 1, adhesion in biological systems is achieved by either friction, bonding, or interlocking, each acting across different biological scales [2]. Friction encompasses

microscale interlocking between an organism and a surface. Bonding includes chemical adhesion, suction, and capillary adhesion. Interlocking, unlike friction, occurs on a macroscopic scale and is achieved by the use of digits or hooks to catch onto protrusions or penetrate into a surface.

Table 2.1: Scales and mechanisms of adhesion in clingfish.

Scale	Friction	Bonding	Macro-Interlocking
MACRO	○	● A ● B	○
MICRO	● C	● D	○

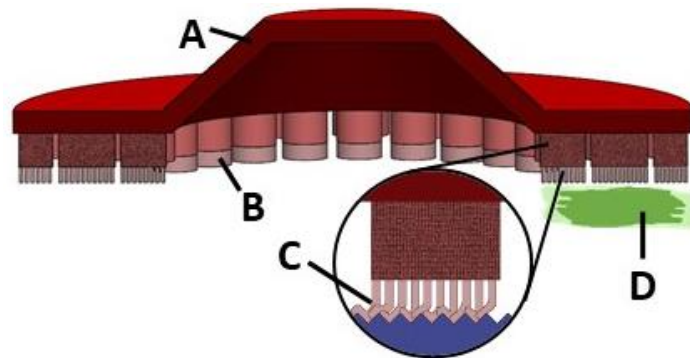


Figure 2.2: Overview of the biological mechanism of adhesion in the clingfish, corresponding to Table 2.1. **A** Suction chamber, for bonding via suction. **B** Pad, for capillary adhesion. **C** Fibrils, for friction and micro-scale interlocking. **D** Secretions, for aiding in capillary and chemical adhesion.

As detailed in Table 2.1 and Figure 2.2, the clingfish accomplishes adhesion on both micro- and macroscopic scales, through bonding and friction. On the macroscopic scale, the suction chamber is used for bonding by creating a low-pressure chamber. The pads also aid in

bonding by providing a mechanism for capillary adhesion. On the microscopic scale, the fibrils are used for increasing the frictional footprint of the clingfish. By microscopically interlocking to the irregularities of a surface, the fibrils resist slip of the disc margin and seal the inner suction chamber. Lastly secretions were investigated for their role in chemically adhering to a surface. After our investigations, we concluded that the secretions do not play a large role in chemically binding to a surface, but do contribute to adhesion via capillarity. In sum, the mechanisms of adhesion of the clingfish are hierarchical in complexity. Suction, capillarity, and friction act on both micro- and macroscopic scales to successfully adhere the clingfish to rough substrates.

2.1 Experimental Set-Ups

2.1.1 Sample collection and preparation

Live clingfish were collected along the San Diego coastline. Permit to Scripps collector, Phil Zerofski. Animal care protocol IACUC #S11071. Experiments involving fresh tissue samples were performed day of animal sacrifice.

Preserved clingfish samples were obtained from the Scripps Marine Vertebrate Collection. Specimen were preserved in 70 percent ethanol.

2.1.2 Imaging techniques

Fresh and preserved tissue samples were imaged under brightfield microscopy (Carl Zeiss AG, Germany) using a SMZ1500 Nikon camera.

Clingfish from the Scripps Marine Vertebrate Collection were imaged under the Scanning Electron Microscope FEI Apreo SEM (Thermo Scientific, USA). The anterior disc margin was analyzed during SEM.

Fresh tissue samples were preserved in 70 percent ethanol and imaged under Transmission Electron Microscopy using the FEI Tecnai Spirit G2 BioTWIN Transmission Electron Microscope (Thermo Scientific, USA).

The setup for Frustrated Total Internal Reflection (FTIR) experiments was custom-built in accordance to (Han 2005). The station was constructed with a 3D printed mount, clear acrylic, and infrared LEDs. The light emitted from the diodes was internally reflected within the acrylic. Contact with the acrylic plate allowed for the illumination of the surface.

2.1.3 Pull-tests

Fresh tissue samples were interrogated with the Dimension Fast Scan Atomic Force Microscope using a Fastscan-B cantilever (Bruker Nano Inc., USA) of spring constant 1.793 N/m and a manufactured tip radius of 20 nm. All AFM tests were performed in a filtered saline solution. Analysis of AFM interrogations were performed on NanoScope Analysis (Bruker Nano Inc., USA).

Pull tests were performed using the Instron 3342, capacity 500 N. Biological specimen were firmly secured via metal hooks and a clamp to the load cell. Scaled pad analogs were fabricated with handles and clamped into the load cell. The scaled pad analogs were fabricated on the Stratasys Objet350 Connex3.

2.2 The structures of adhesion of the clingfish

2.2.1 The role of the suction chamber

Suction is a large driver of adhesion in the clingfish. In order to understand the theoretical maximum for suction, the clingfish disc was approximated to a suction cup, as illustrated in Figure 2.3.

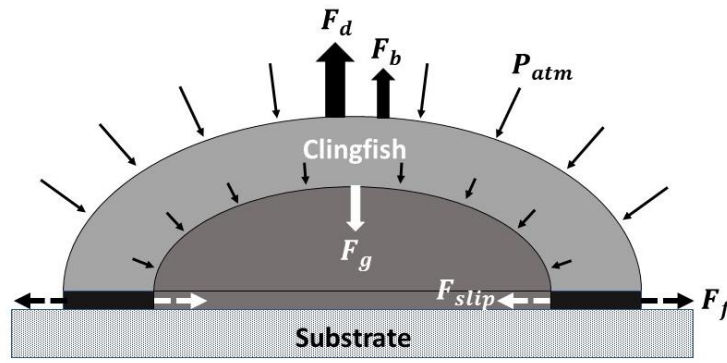


Figure 2.3: Force balance of clingfish suction chamber. The detachment force, F_d , is equal to the force created by atmospheric pressure, P_{atm} . Force due to buoyancy, F_b . Force due to gravity, F_g . Friction (F_f) is lateral force opposing slip (F_{slip}).

The theoretical maximum adhesive force due to suction is given by:

$$F_d = P A \quad (1)$$

The detachment force, F_d , is equal to the pressure, for which we will assume $P = P_{atm}$, and A for the area of the suction disc. We will assume that the contributions of buoyancy (F_b) and gravity (F_g) are negligible. Additionally, we will assume the force of friction (F_f) balances slip (F_{slip}) in the disc margin. Rearranging (1) yields the theoretical maximum of adhesive stress (σ_d) of the suction cup due to atmospheric pressure (P_{atm}) of 101 kPa.

$$\sigma_d = P_{atm} = \frac{F_d}{A} = 101 \text{ kPa} \quad (2)$$

Therefore, the theoretical adhesive stress of an idealized suction cup on a flat, smooth surface is 101 kPa.

In previous studies, the clingfish is reported with an adhesive stress of approximately 25 kPa on smooth surfaces [11], corresponding with pressures of 0.2-0.5 atm below ambient. The inability to achieve the theoretical maximum of suction of 101 kPa suggests that the suction chamber of the clingfish is not a perfect suction cup and experiences leakages in the seal.

Indeed, by removing elements of the disc margin, such as the pads, the adhesive stress of the clingfish is dramatically reduced (Figure 2.4). Prior to the pull tests demonstrated in Figure 2.4, the pads of the clingfish were removed by mechanical abrasion. This particular experiment demonstrated a two order of magnitude difference between the theoretical maximum adhesive stress of the clingfish and the achieved adhesive capabilities.

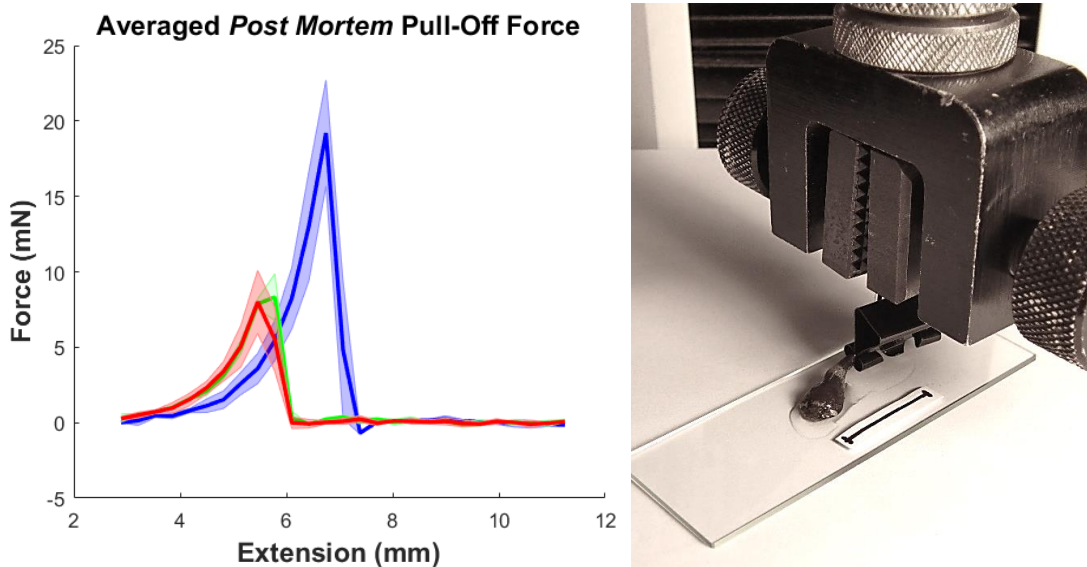


Figure 2.4: *Left* Averaged pull-off force of euthanized clingfish, demonstrated directional adhesion. Clingfish pulled forward 2 cm prior to removal from surface, 3 trials (blue). Clingfish pulled backwards 2 cm prior to removal from surface, 4 trials (red). Clingfish removed from surface without directional pull, 3 trials (green). Rate of removal, 8 mm/s. ***Right* Experimental setup of pull-tests.** Scale bar, 2 cm.

Additionally, the clingfish suction disc chamber itself demonstrates a preference in directionality of loading. As demonstrated in Figure 2.4, the euthanized sample that was pulled forward 2 cm nearly doubled its adhesive force in comparison to when pulled backward or stationary.

The clingfish was analyzed using Frustrated Total Internal Reflectance (FTIR) to monitor points of contact during adhesion. The specimen was live during FTIR experimentation and held upside down to the imaging plate. As demonstrated in Figure 2.5, the clingfish has many orientations of its body geometry to adhere to the experimental surface.

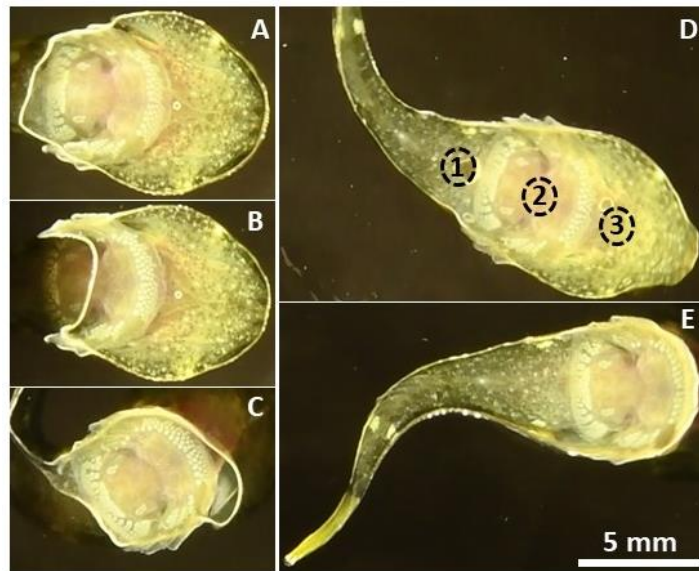


Figure 2.5: Ventral views of the orientations of a live clingfish during adhesion, imaged under Frustrated Total Internal Reflectance. A Disc and head in contact with imaging surface. Two suction chambers created. **B** Anterior disc margin and head in contact creating one cavity. **C** Only suction disc engaged with imaging surface. One cavity formed. **D** Body of clingfish in complete contact with imaging surface. Three cavities formed (1-3). **E** Complete disc and posterior body in contact with surface. Two cavities formed.

In all but one scenario, the suction disc is fully engaged. For the case during which the suction disc was not fully engaged (Figure 2.5B), only half of the disc margin was in contact

with the imaging plate. The finned region of the disc margin provided a mechanical support much like a brace, while the space between the anterior disc margin and the mouth acted as a suction chamber. This combined effect allowed for the clingfish to maintain adhesion although the suction disc was disengaged. It is apparent in Figure 2.5 D, labels 1-3, that the clingfish has three significant depth levels along the ventral side of its body. The first and most apparent cavity formed is the chamber of the suction disc itself, which is created by the union of the modified pelvic and pectoral fins. The second and third cavities formed are anterior and posterior to the suction disc (Figure 2.5 D). Thus, three suction chambers are formed when the whole ventral surface of the clingfish is in contact with a substrate. However, for the purposes of this investigation, we will focus solely on the central suction disc. From this experiment, it also became apparent that the margin of the suction disc is raised from the continuity of the body and that the disc itself can be reversibly disassociated from the main body. This disassociation provides a greater degree of freedom in the response of the disc to variable stimuli.

The disc margin performs a crucial role in maintaining the isolation of the suction chamber. Upon gentle prodding at the intersection of the pelvic and pectoral fins (Figure 2.6 A), the seal of the suction chamber was compromised (Figure 2.6 B). During the separation of the fish from the imaging surface, the pads remain in contact with the plate for the greatest duration of time post-rupture of the low-pressure chamber.

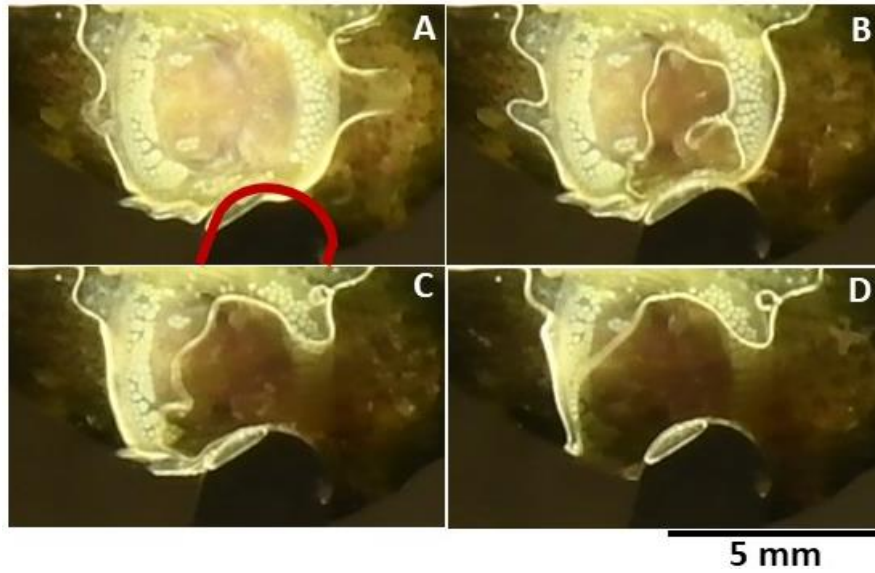


Figure 2.6: Time series of a disassociation event. **A** The intersection of the pelvic and pectoral fins was gently prodded with a rounded probe, outlined in red. **B** The pressure of the chamber increases to ambient pressures. **C-D** Progressive disassociation of clingfish disc margin.

2.2.2 Characterization of the pads

It is apparent from the FTIR trials that the interdigitated pad structures covering the disc margin contribute to the process of adhesion. In order to understand the role of these pads to adhesion, we first investigated the total surface area covered by the pads. Using microscopy and custom image processing algorithms, we were able to stitch together high magnification images to create a map of the pads. The pads were then automatically identified and measured for such parameters as their area and eccentricity.

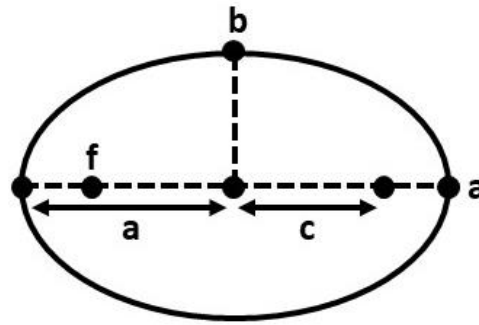


Figure 2.7: Eccentricity of an ellipse. *a*: semi-major axis length. *b*: semi-minor axis length. *c*: distance from the center to foci, *f*.

Eccentricity (*e*) is defined as the ratio of the distance (*c*) between the foci (*f*) and center of an ellipse to its semi-major axis length (*a*) (Figure 2.7). The distance between the foci can be derived from the minor axis length (*b*) (Eq 3).

$$e = \frac{c}{a} = \sqrt{1 - \left(\frac{b}{a}\right)^2} \quad (3)$$

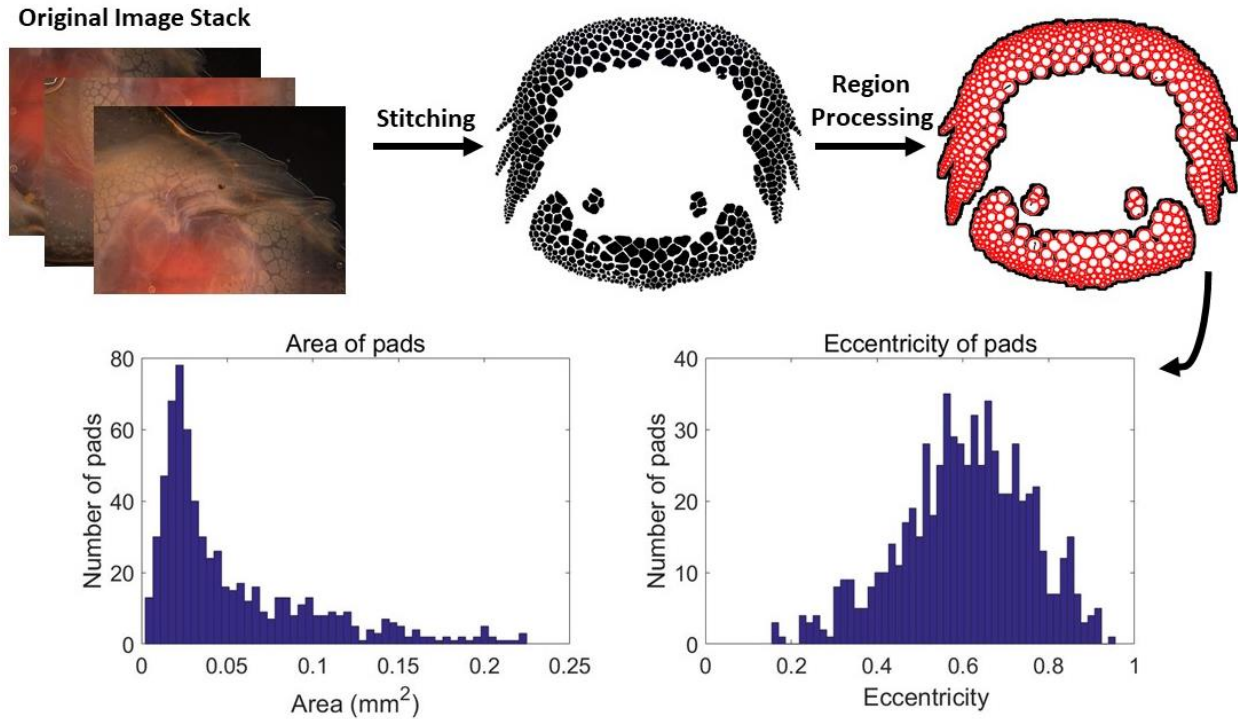


Figure 2.8: An overview of the image processing procedures to generate a high-resolution map of the pads of the disc margin. Left to Right High magnification images were stacked and stitched together using a custom-built algorithm. The resulting map, presented as a black and white figure, was then run through a region processing algorithm that measured a variety of characteristics of the pads, including the area and eccentricity of each individual pad. These characteristics are presented as histograms.

The following trends arose from this image processing procedure. The first was that the amount of small pads ($<0.1 \text{ mm}^2$) greatly outnumbered the amount of large pads. The map of the pads presented in Figure 2.8 shows the highest densities of small pads near the outer edge of the disc margin.

The distribution of pad eccentricities on the histogram of Figure 2.8 was that of a Gaussian centered on a mean eccentricity value of 0.60 with a standard deviation of 0.15. The mean eccentricity of the pad is therefore elliptical, as opposed to circular for which the eccentricity would be zero. The patterning of the pads along the disc margin and the interlocking nature of the ellipse shapes perhaps aid in the channeling of water from the inner pressure

chamber when the disc comes into contact with a surface. The interdigitation therefore would act to conform to a surface and during suction, would act as a mechanism to lock to the contours of the substrate.

The significant surface area of the pads across the footprint of the suction disc suggests that these structures serve an important role in adhesion. We further investigated the pads by a combination of microscopy techniques.

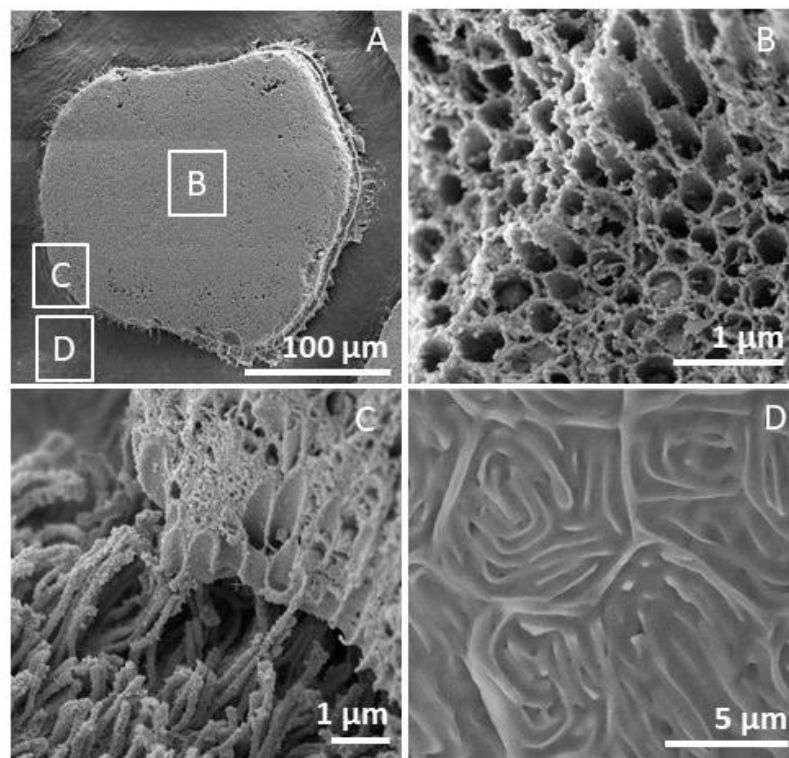


Figure 2.9: Scanning Electron Micrographs of pad on disc margin reveal extensive microchannel network. **A** Single pad on the disc margin. **B** The entirety of the surface of the pad is an elaborate system of microchannels with an average diameter of 0.25 μm. **C** A fracture along the edge of the pad reveals soft fibrillar extrusions that tunnel through the microchannels to be expressed on the pad surface. **D** Cuboidal epithelium characteristic of teleost fishes. SEM performed on preserved sample from Scripps Marine Vertebrate Collection.

Scanning Electron Microscopy (SEM) of preserved samples from the Scripps Marine Vertebrate collection reveal an extensive network of microchannels expressed at the surface of each pad (Figure 2.9 B). These microchannels extend across the entirety of the ventral face of the pad. The microchannels act as tunnels for soft fibrillar extrusions, as seen on the fractured edge in Figure 2.9 C. These fibrillar extrusions are shown to project through the microchannels, and are hypothesized to be expressed on the surface of the pad. These extrusions, referred to in previous works as papillae, had been described to be rod-like [11]. However, in order to avoid this unintended connotation of rigid rods, the term fibrillar extrusion will be used for the remainder of the work presented in this and the following chapters.

Transmission Electron Microscopy (TEM) of a pad further supports the observation of an extensive microchannel network to express soft fibrillar extrusions at the surface.

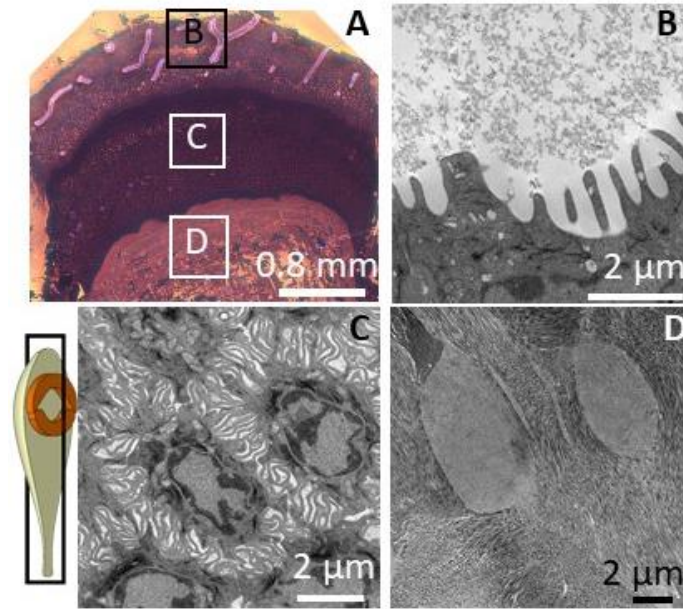


Figure 2.10: Transmission Electron Micrograph of a pad. **A** A semi-thin tissue section was prepared. Three distinct layers of tissue are distinguishable. Orientation of cuts indicated by the clingfish schematic in the lower left-hand corner. **B** Microchannels are expressed on the surface of the pad. Average diameter of channel $0.25\ \mu\text{m}$ at a spacing of $0.02\ \mu\text{m}$. **C** Microchannels continue below the surface of the pad, forming a hexagonal network of intersecting channels. This network extends for a depth of 1 mm across the cross section of the pad. **D** Muscle fibers in many orientations suggest dynamic response to stimuli.

TEM reveals that the network of microchannels extends for millimeters below the surface of the pad. The microchannels were measured on the surface of the pad to have an average diameter of $0.25\ \mu\text{m}$ and are spaced $0.02\ \mu\text{m}$ apart. Below the surface, the microchannels broaden to a diameter of $1\ \mu\text{m}$ and intersect neighboring channels in a hexagonal fashion. The change in the diameter of the channels from $1\ \mu\text{m}$ in the body to $0.25\ \mu\text{m}$ at the surface suggests that the fibrillar extrusion is soft and compliant in order to navigate the microchannel network. The folds in the channels are hypothesized to be nascent fibrils to be later expressed on the surface of the pad (Figure 2.10 C). The orientations of the bundles of muscle fibers in Figure 2.10 D allows for a dynamic, controlled response of the clingfish to random stimuli.

2.2.3 The role of the fibrils

The fibrils described in Section 2.2.2 as extrusions extending from the pad surface are hypothesized to be compliant. Fibrils imaged in SEM micrographs lack a consistent orientation, which would be expected in an adhesive structure, such as the directional setae of the gecko. In organisms that rely on microstructures for adhesion, such as the gecko, the orientation of the setae is consistent across the foot pads. The non-homogenous orientation of the fibrils thereby suggest that the microstructures are not intended for adhesion as the setae of the gecko, but rather serve to seal surface irregularities.

In order to test this hypothesis, the surface of the pads was interrogated by Atomic Force Microscopy (AFM) on a fresh tissue sample in a droplet of filtered sea water. The tissue was left unaltered prior to experimentation, thus leaving undamaged the fibrils and the associated secretions. All tissue samples and isolated secretions remained hydrated in a saline solution for the entirety of the experimental procedure. The AFM tip tested the adhesive strength of the fibrils and secretions that had been isolated from the same euthanized specimen. Unbinding events are observed in Figure 2.11 C as sharp vertical transitions in the unloading force curve.

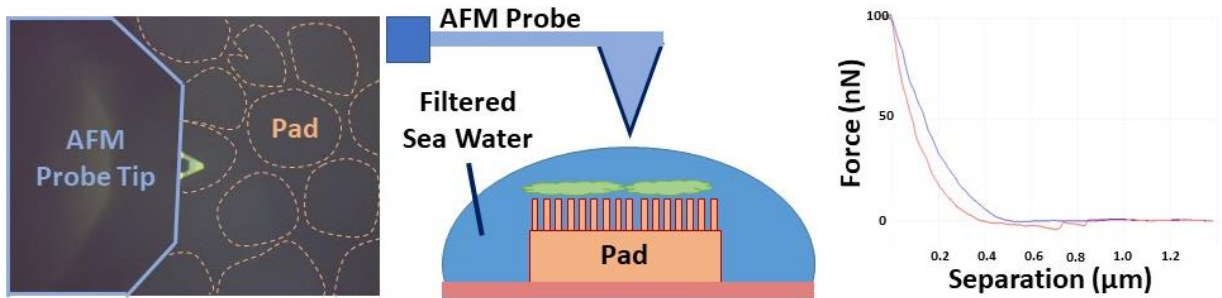


Figure 2.11: Atomic Force Microscopy to determine adhesive strength of fibrils and secretions. **A** View of probe tip over pad. **B** Setup of AFM measurement occurred in droplet of filtered sea water as to hydrate the sample. **C** Example force curve with two unbinding events.

AFM revealed that the secretions were roughly three times less adhesive than the fibrils. The fibrils themselves varied in their force of adhesion based on location. The finned regions of the clingfish had lower pull-off forces than the pads located on the anterior disc margin. The secretions had an average force of 0.5 nN (18 samples), while the anterior disc margin and fins were measured at an average force of 1.75 nN (30 samples) and 1.42 nN (26 samples), respectively.

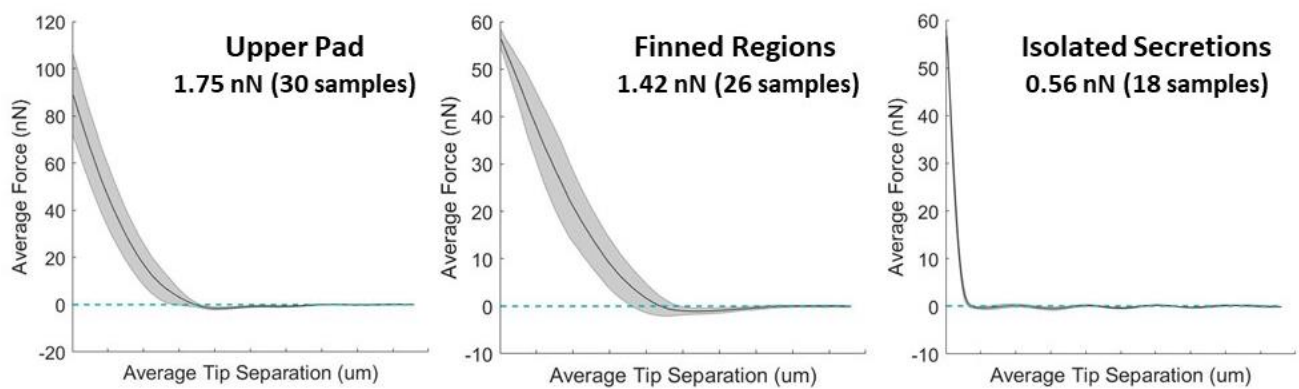


Figure 2.12 Average force (nN) of adhesion for regions of the clingfish pad. **A** The upper pad refers to the anterior disc margin, which had the largest force of adhesion. **B** Finned regions refers to the pads on a fin of the disc margin. **C** Secretions were isolated and vortexed prior to interrogation by AFM.

Given that the interrogation of the pads occurred with secretions present (Figure 2.11 B), one can subtract the contribution of secretions from the reported adhesive forces for the anterior disc margin and fins. The average pull-off forces of 1.25 nN and 0.92 nN result for the anterior disc margin and fin pads without secretions present.

The AFM probe has a conical tip with a manufactured radius of 20 nm and a spring constant of 1.795 N/m. However, SEM imaging of the tip was not performed after the interrogation of the sample. Therefore, the area of the probe tip in contact with the fibrils was not adequately measured, leading to uncertainty in the calculations of adhesive stress, in which the adhesive force is related to contact area. Assuming that the tip end is hemispherical with a radius of 20 nm, the average stress of adhesion of the fibrils of the anterior disc margin and fin (without contribution of secretions) and isolated secretions are 124 kPa, 91 kPa, and 55 kPa, respectively. However, as the probe tip was worn from previous experiments, the tip radius may have increased due to wear. Assuming that the tip radius increased to 30 nm, the average stress of adhesion of the anterior disc margin, fin, and isolated secretions are 55 kPa, 40 kPa, and 24 kPa, respectively. Thus, the probe tip geometry effected the calculation of the adhesive stress, making it a less reliable estimation of the adhesive stress of the fibrils. As a comparison, adhesion values of geckos are reported at 576 kPa [17] and 240 kPa for the spider, *E. arcuata* [4]. The adhesive stress of the clingfish fibrils is therefore roughly an order of magnitude less than those of gecko and spider microstructures. This suggests that the fibrils are not the primary mechanism of adhesion of the clingfish. The low values of adhesive stress of the isolated secretions verified the hypothesis that the secretions are used for sealing, not for chemical adhesion to surfaces.

2.2.4 Capillary adhesion estimation with scaled pull-tests

The role of secretions

One common mechanism of underwater adhesion by marine organisms is via chemical bonds. One example is the protein secretions of the marine mussel which result in strong adhesion to underwater surfaces [18]. Echinoderms also attach and detach their tube feet to surfaces using adhesive and de-adhesive secretions [19]. These are two examples in which the secretions are necessary for chemically binding and adhering the organism to an underwater surface. This is not the case in the northern clingfish. The isolated secretions coating the clingfish pad are three times less adhesive than the fibrils of the clingfish when interrogated by AFM in a saline solution. The primary driving mechanism of clingfish adhesion is not via chemical binding. However, the contributions to adhesion of the secretions cannot be overlooked nor understated.



Figure 2.13: Secretions present on dried clingfish footprint. **A** View of clingfish footprint on a glass slide, imaged under Brightfield microscopy. **B** Glycoprotein ferning patterns evident along suction disc margin. **C** Geometric shape and orientation of secretions.

Secretions in the clingfish were hypothesized to 1) help seal the suction disc on irregular surfaces and 2) increase the effect of Stefan adhesion. Although suction by the empty chamber is the primary mode of adhesion in the clingfish, sealing the disc margin is just as integral to the success of the clingfish. Secretions are also more viscous in comparison to sea water and therefore increase the contribution of Stefan adhesion to total adhesion. In this case, Stefan adhesion is the normal stress acting between the clingfish pads and a surface during separation.

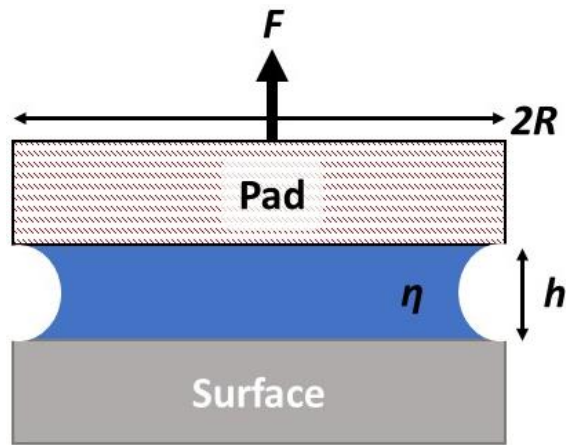


Figure 2.14: Stefan Adhesion acting between two parallel plates when separated. Plates of radius R , fluid of viscosity η .

$$F = \frac{3\pi\eta R^4}{2h^3} \frac{dh}{dt} \quad (4)$$

Stefan adhesion is the normal stress (F) acting between two parallel plates with a radius of R and at a separation distance of h . The plates are separated from each other at a rate of $\frac{dh}{dt}$ in a fluid of viscosity η . The clingfish pads are approximated to a circular plate, pulled from an equally flat surface. In accordance to Equation 4, the adhesive strength of the parallel plate

system is linearly proportional to viscosity of the medium. Water has a viscosity of $1.234 \text{ mPa} \cdot \text{s}$ at 12°C whereas fish skin mucus of teleost fishes has a viscosity of between 2 and $3 \text{ mPa} \cdot \text{s}$, the variation being species dependent [20]. Thus, the adhesive force of the clingfish will be greater with secretions than without. However, the estimation of the viscosity of the secretions was based on the values of fish skin mucus, which may differ from the secretions from the clingfish pad itself.

A scaled adhesion test was performed in order to verify this hypothesis as to the role of secretions. In order to do so, the geometry of a clingfish pad was scaled by a factor of 50 and pulled from a surface submerged in a bath of glycerol. Mineral oil, with a viscosity of $55 \text{ mPa} \cdot \text{s}$, is an analog to sea water when the viscosity is scaled by a factor of 50. The adhesive stresses in glycerol were compared to the adhesive stresses in glycerol, viscosity of 1.412 Pa , which acted as an analog for secretions when the viscosity is scaled by 50.

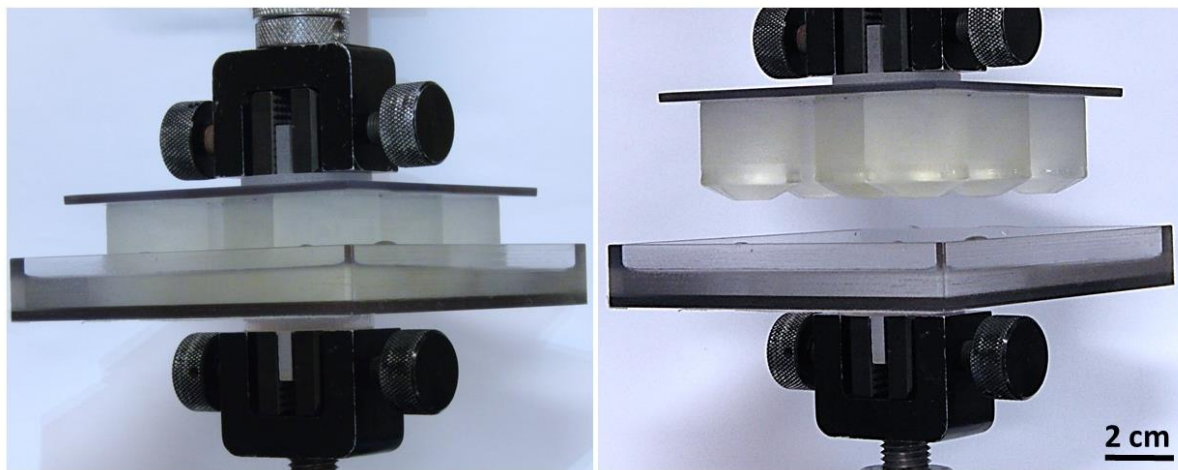


Figure 2.15: Scaled adhesion experiment to test contribution of Stefan adhesion to total adhesive capabilities of the clingfish. A Pad array in contact with flat surface in a bath of glycerol. **B** Array of pads pulled perpendicular from surface and the adhesive stress was calculated.

The pads themselves were designed using measurements from TEM micrographs and scaled up by 50. The scaled pads were 3D printed using the Stratasys Objet350 Connex3. The pad analog was a combination of three stiffnesses and materials, the most compliant at the outer surface of the pad and the stiffest towards the backing (Figure 2.16). We measured the adhesive stress of the pad array using the Instron 3342. The pad geometry was also varied. As observed in the TEM micrograph, the pad has a tapered angle of 25 degrees, which propagates throughout the cross-sectional depth of the pad. In order to investigate the effect of this taper, which reduces the area in contact with a surface, the geometry was compared to an array of pads with only a flat surface of an equivalent surface area.

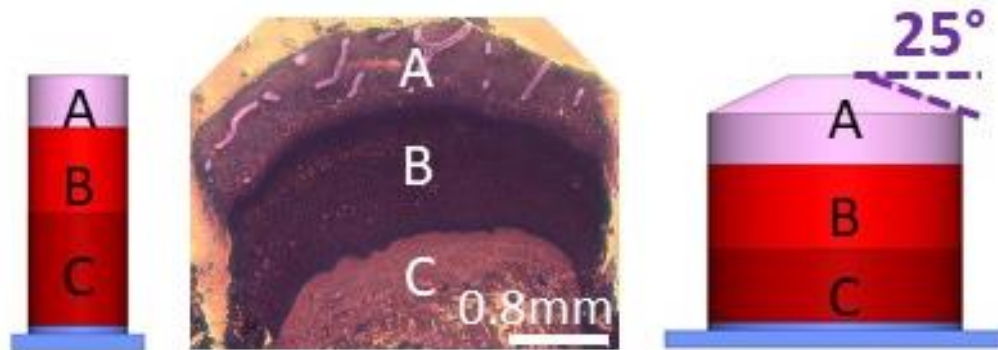


Figure 2.16: Geometries of scaled array of pads for tests of Stefan adhesion. Computer renderings of scaled pads with three stiffness, pink being the most compliant and dark red being the least. Based on analysis of TEM micrographs (center).

Contrary to our initial hypothesis, the more viscous fluids only improved the adhesive force at higher pull-off rates. Although there was a difference in the average pull-off forces of the filleted pads in mineral oil versus glycerol at a rate of 0.5 mm/s, this was reversed for the slower speed of retraction. Thus, these findings suggest that the secretions are most valuable to a clingfish during rapid disturbances, such as wave surges. Otherwise the secretions play less of a role in adhesion when disturbances are less impulsive.

Table 2.2: Averaged adhesive force of scaled pads versus speed of retraction

Speed of Retraction	Mineral Oil	Glycerol
0.5 mm/s	5.3 N	7.9 N
0.2 mm/s	6.1 N	5.9 N

The 25-degree tapered edge on the clingfish pad reduced the adhesive force at all but moderate speeds in comparison to the pads without a taper. This performance is consistent across preloaded and non-preloaded trials (Figure 2.17). Additionally, a preload of 10 N magnified the adhesive force of the filleted and non-filleted pads by a factor of 10.

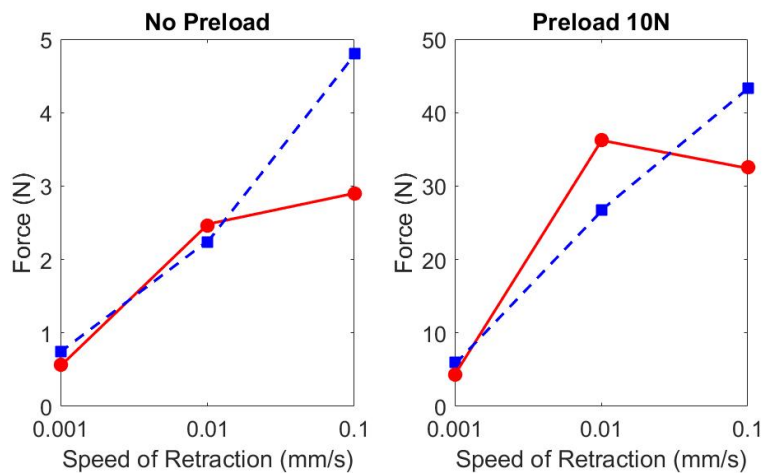


Figure 2.17: Fillets affect adhesive force of scaled pads and is rate dependent. Non-filleted pads, blue square. Filleted pads, red circle. Speed of Retraction: Slow (0.001 mm/s), Moderate (0.01 mm/s), Fast (0.1 mm/s). Note the difference in y-axis scale.

The reduced performance of the filleted pads at high speeds could be due to a number of different factors. One hypothesis is that fluid accumulates at the fillet edge that is then pushing against the surface from which the pads are being removed. This repulsion is emphasized at high rates of retraction and decreases the pull-off force.

Additionally, the filleted pads experienced two abrupt changes in adhesive force (Figure 2.18) in comparison to the non-filleted pads. This suggests that two disassociation events occurred before the pads were entirely removed from the surface. The two dissociation events implies that the fluid adhered to the fillet walls of the pad, in addition to the face parallel to the pull-off surface. This phenomenon was consistent in slow and moderate speeds of retraction for only the filleted pads.

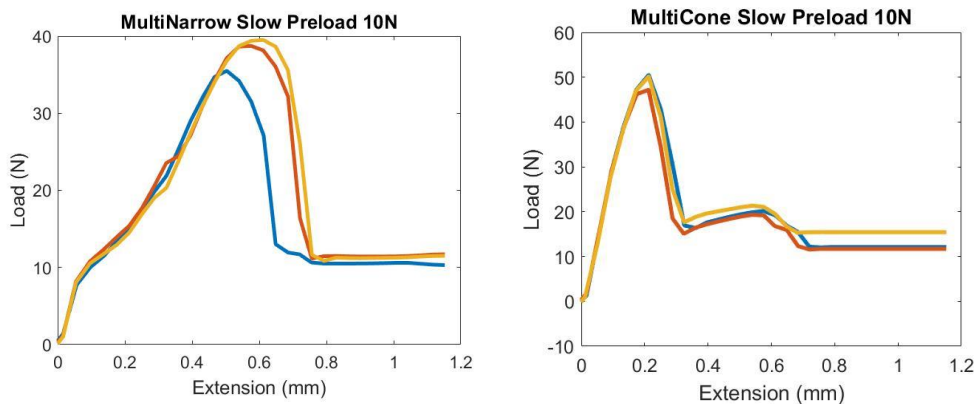


Figure 2.18: Example raw data adhesive force curves: Fillets with two disassociation events. Left Non-filleted pads. **Right** Filleted pads. Speed of Retraction: Moderate (0.01 mm/s). In both figures, pads were preloaded to 10N.

2.3 Conclusion

The mechanisms of adhesion in the clingfish are complex and hierarchical. The main driver of adhesion in the clingfish is suction which is a difference in pressure between the external fluid and the inside of the suction disc. The disc margin surrounding the suction chamber is integral in sealing the internal chamber. The structures of the disc margin, namely the elliptical pads and their network of fibrils, serve to seal the chamber and are not the main driver of adhesion alone, as investigated with the AFM. The hollow tube structures on the surface of the pad act as a pathway for soft extrusions to be expressed on the surface. This finding adds an alternative definition and classification of the papillae from a network of “rods” to a network of extrusions that do not have a specified orientation.

The network of extrusion microchannels are extensive, accounting for approximately 600 μm of the thickness of the clingfish pad. They serve as a mechanism to seal the internal pressure chamber of the clingfish, and are non-homogenous in their orientation. The secretions act to further seal the suction chamber, given their low adhesive strength under AFM investigations. Additionally, secretions and pads aid in adhesion via capillarity, as explored in scaled Stefan adhesion tests. The clingfish achieves adhesion by bonding on the macroscale and friction on the microscale. The methods of bonding are driven by suction and capillarity, with minor contributions of chemical binding. Friction is governed by the microinterlocking mechanisms of the soft fibrils. Overall, the complex hierarchy of adhesion can be distilled to the use of compliance to conform to the irregularities of a surface and seal a suction chamber.

Chapter 2, in part is currently being prepared for submission for publication of the material. Sandoval, Jessica; Quan, Haocheng; Meyers, Marc A.; Tolley, Michael T.; Deheyn, Dimitri D. "The hierarchical mechanisms of adhesion of the suction disc of the northern clingfish". The thesis author was the primary investigator and author of this material.

Chapter 3

A biomimetic suction disc:

Design and performance of clingfish-inspired adhesive technology

The biological investigations of the hierarchical structures of adhesion of the clingfish suction disc led to the development of an artificial analog. The artificial suction disc maintained suction on rough and granular surfaces and on planar and non-planar body geometries. The clingfish-mimic, weighing 2.3 grams, was capable of bearing a load on a rocky surface that totaled 1.65 lbs.

3.1 Mechanisms to mimic

As presented in Chapter 2, the mechanisms of adhesion of the clingfish are complex and hierarchical. However, the mechanisms can be generalized to the following roles. First, the

pelvic girdle of the clingfish serves to provide a chamber for sub-ambient pressure (Figure 3.1 A). The pelvic girdle, although compliant to conform to variable surfaces is still sufficiently stiff to resist the slippage of the disc margins to the center and essentially cause failure of the suction disc under low adhesive stresses. The second mechanism is the act of sealing the low-pressure chamber in conformation to surface textures. The dense array of soft fibrillar extrusions serves to fill the rough surface irregularities and increase friction to oppose the buckling of and failure in the clingfish disc under normal stresses (Figure 3.1 C). The secretions were also shown to have low adhesive strengths and thus also contribute to sealing the suction chamber.

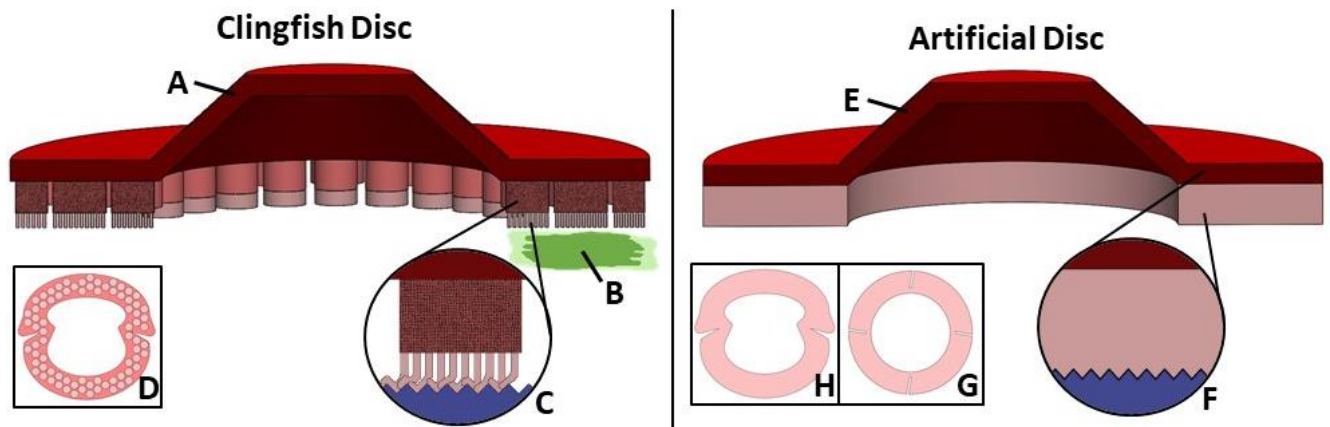


Figure 3.1: Clingfish suction disc inspires structure and material properties of an artificial suction disc. **Left** Overview of the hierarchy of adhesion of the clingfish suction disc. **A** Intricate muscle network for dynamic control of suction disc. **B** Secretions for sealing internal low pressure chamber. Atomic Force Microscopy measurements suggest non-adhesive role of secretions. **C** Cross-sectional view of individual pad. Soft fibrillar extrusions are expressed at pad surface from microchannel network. Extrusions comply to a surface to create a seal. **D** Ventral view of cling fish suction disc. Circles represent individual pads. **Right** Overview of the structure of the artificial suction disc that was inspired by that of the clingfish. **E** The low-pressure chamber composed of Dragon Skin 20 silicone. **F** Ecoflex 00-30 silicone lines the perimeter of the suction chamber. The Ecoflex 00-30 silicone acts as a soft compliant layer to seal low pressure internal chamber of suction disc. **G** Ventral view of most successful artificial suction disc shape, which consists of a circular footprint with four radiating slits. **H** Ventral view of the artificial suction disc using the geometries of the footprint of the clingfish.

The artificial disc therefore mimics the mechanisms of sealing in order to successfully grab onto and seal irregular surfaces and shapes. First, the low-pressure chamber of the artificial disc was composed of Dragon Skin 20 (Smooth-On, Macungie, PA, USA), a stiff silicone of shore hardness 20A. The material, although elastic enough to conform to non-planar geometries, was stiff enough to resist significant deformation and slippage inwards when a stress normal to the surface was applied. Secondly, the fibrillar extrusions were approximated to a layer of soft silicone, Ecoflex 00-30 (Smooth-On, Macungie, PA, USA). The soft silicone filled the irregularities of the surface and sealed the low-pressure chamber. The process of conforming to the texture of the surface resulted in an increase in friction of the disc margin to prevent slippage towards the center of the disc.

The artificial disc also mimicked the geometry of the clingfish (Figure 3.1 G, H). The incorporation of slits into the disc margin resulted in a greater resistance to normal stress applied to the disc, and thus was able to bear a larger load. However, although the clingfish is bilaterally symmetric, the most successful prototype iteration was radially symmetric. These conclusions and design considerations are further explored in the following sections.

3.2 Fabrication of the artificial suction discs

Artificial suction discs were fabricated using molds that were 3D printed on the Stratasys Objet350 Connex3. Body geometries were either circular, or in the geometry of the clingfish suction disc in accordance to analysis performed by Image J (National Institutes of Health, <http://rsbweb.nih.gov/ij/>) (Figure 3.2).

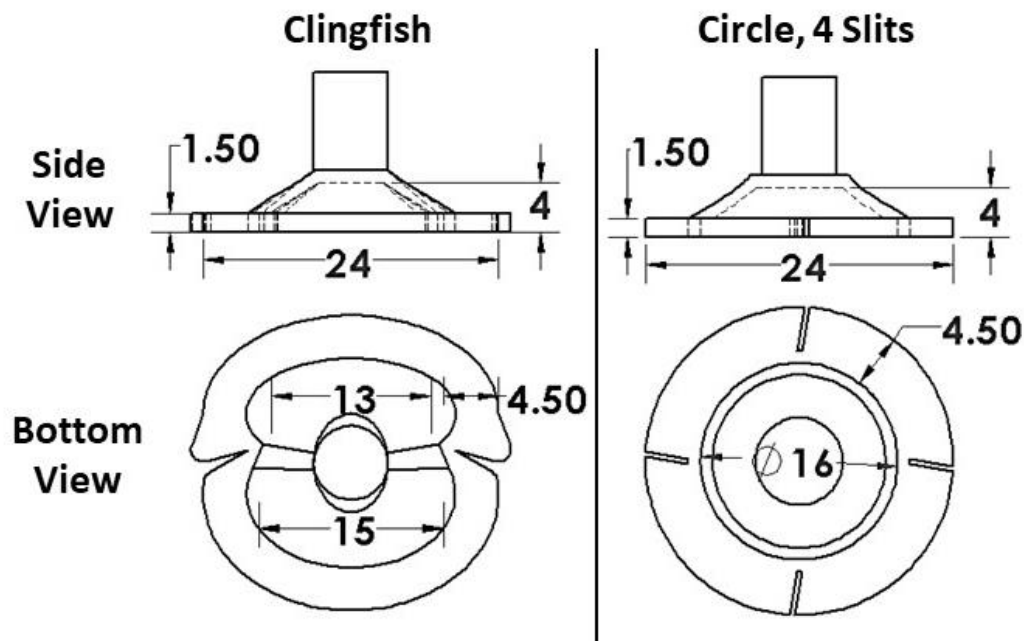


Figure 3.2: Geometries of suction disc low-pressure chambers. Left Clingfish body cavity geometry. **Right** Circular body cavity with four slits. All units in millimeters.

The number of slits in the body cavity walls was also varied to demonstrate the effect of the slit on the performance of the disc on non-planar surfaces. A slit was a cut made in the disc margin of the suction disc. The cavities were molded with cylindrical handles of DragonSkin 20 that were 10 mm in height to provide a gripping surface during tests of disc performance.

The body cavity of each suction disc was entirely composed of Dragon Skin 20. The resulting disc was then coated with a 2 mm layer of Ecoflex 00-30.

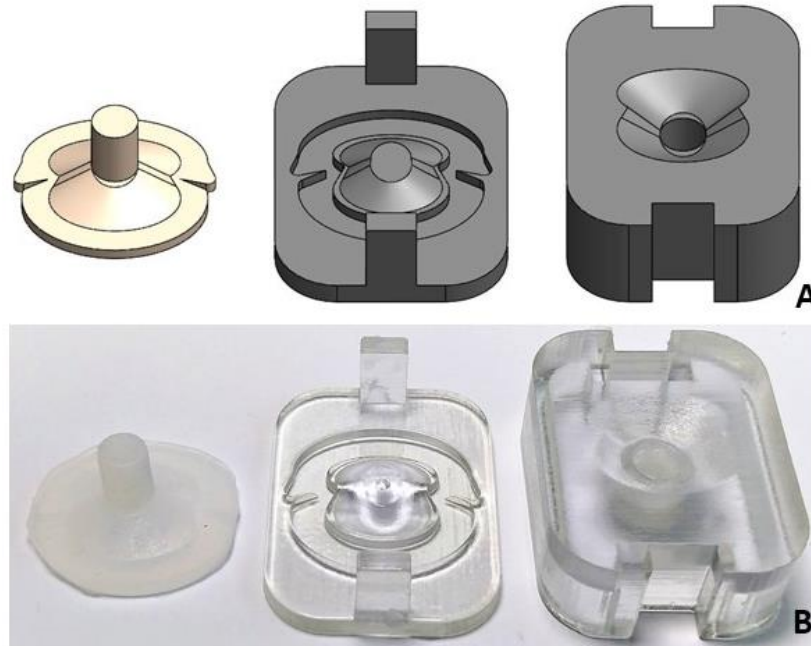


Figure 3.3: Fabrication of low pressure chamber. **A** Computer Aided Design (CAD) model of the mold of the suction disc. **B** Mold 3D printed on the Stratasys Objet350 Connex3. Suction disc (left) molded with DragonSkin 20.

A total of five prototype variants were fabricated and evaluated in order to optimize the design of the artificial disc. The effects of a soft layer, slits, and body symmetry were explored in the prototype variants (Figure 3.4).

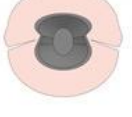
		Soft Layer	Slits	Radial Symmetry
<i>4 Slit with Ecoflex</i>				
<i>No Slit with Ecoflex</i>				
<i>No Slit, No Ecoflex</i>				
<i>Slit, No Ecoflex</i>				
<i>Slit with Ecoflex</i>				
<i>Commercial Suction Cup</i>				

Figure 3.4: Prototype variations. Left are computer renderings of the prototype. Green circles indicate that the feature is present in the prototype. Soft layer is a 2 mm layer of Ecoflex 00-30. Slits are cuts made in the disc margin. Symmetry was either radial (circular) or bilateral (mimic of fish geometry).

3.3 Evaluation of suction disc performance

3.3.1 Maximum normal stress:

Experimental Setup

The suction discs were evaluated by their maximum load supported on naturally-occurring rocky surfaces. These surfaces included a concave fracture of a granite rock, convex exterior of a granite rock, convex smoothed river rock, and flat cratered volcanic rock. The stone was fixed using epoxy to a brass bar. A suction disc, which was fixed vertically, adhered to the stone and suspended in air. Brass weights were incrementally applied to the brass bar until failure of the suction disc. The weight was recorded.

We also evaluated the performance of the suction discs on various substrates using the Instron 3342 (capacity 500 N). We then evaluated the performance of a commercially available suction cup, Hillman model #701477 (capacity 0.5 lbs, diameter 1.25 inches), to provide a comparison to the artificial suction discs. The suction discs were fixed to the Instron by means of a clamp and pulled perpendicular from a secured surface. The maximum adhesive stress was calculated using the force at which the disc failed. All surfaces were submerged in a bath of water for the duration of the pull tests. Suction was induced by pressing the body of the suction disc to the surface, displacing water and creating a low-pressure chamber. Pull tests were performed in triplicates per substrate type. Maximum adhesive stress (σ) was calculated from the maximum pull-off force (F_{ad}) and the surface area of the artificial adhesive disc (A).

$$\sigma = \frac{F_{ad}}{A} \quad (5)$$

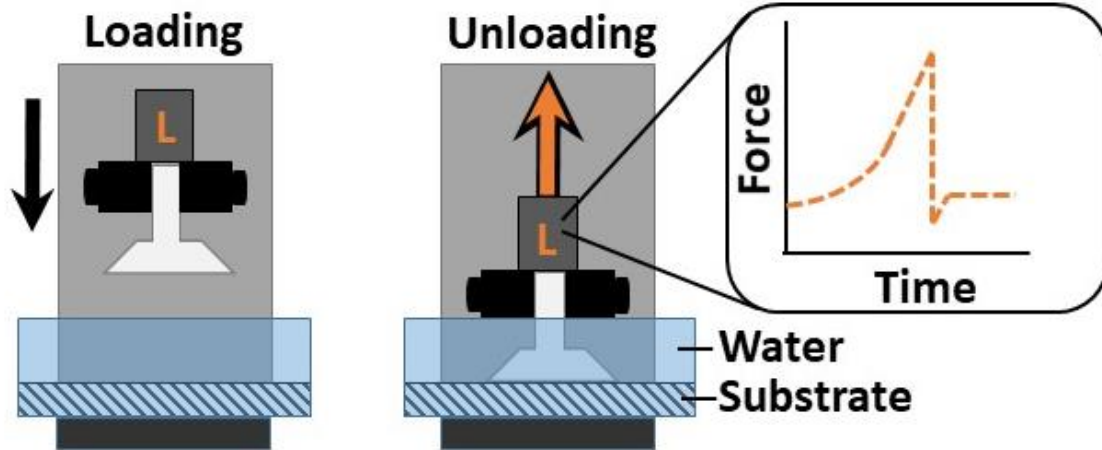


Figure 3.5: Setup of adhesive stress tests performed on the Instron 3342. The substrate was submerged in a body of water. Unloading at constant rate. The load cell, L, records the force and extension, which can be used to calculate force and time curves.

To determine the effects of surface roughness on disc performance, an experimental surface was fabricated with three possible roughnesses: grain sizes of $0\ \mu\text{m}$ (smooth), $68\ \mu\text{m}$ (intermediate roughness), and $269\ \mu\text{m}$ (roughest). The rough experimental surface was fabricated by bonding sandpapers of grits P60 (grain size $269\ \mu\text{m}$) or P220 (grain size $68\ \mu\text{m}$) to an acrylic plate using double-sided adhesive (3M, USA). The smooth experimental surface consisted of an acrylic plate.

To determine the effects of surface geometry and concavity on disc performance, an experimental surface was fabricated with halved PVC pipes of diameters: 70 mm, 56 mm, 50 mm, 33 mm, and 20 mm (Figure 3.6). A concave surface was generated by the inner wall of the PVC pipe. The convex surface was represented by the outer wall of the tube.

To determine the combined effects of surface concavity and roughness, an experimental surface was fabricated with halved PVC pipes that were then bonded to with sandpapers of grits P60.

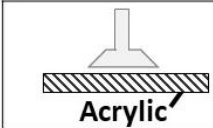
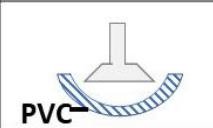
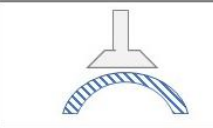
	Flat	Concave	Convex
Smooth			
Rough			

Figure 3.6: Setup of surfaces on which pull tests were conducted. Surface roughness experiments were tested on flat plates. Concavity experiments were tested on halved PVC pipes. The combination of the effects of concavity and texture was evaluated on PVC with sand paper adhered to the surface.

3.3.2 Frustrated Total Internal Reflection of the disc foot print

Experimental Setup

The area of contact of the suction disc was investigated using Frustrated Total Internal Reflection (FTIR). The setup of the FTIR imaging station was a custom set up in accordance with protocol established by Han 2005. The station was constructed with a 3D printed mount, clear acrylic, and infrared LEDs. The light emitted from the diodes was internally reflected within the acrylic. Contact with the acrylic plate allowed for the illumination of the surface area in contact. A camera filmed from above the acrylic plate. The suction disc was attached from the bottom of the acrylic plate, and manually pulled perpendicular from the surface to understand the failure mode of the suction disc.

3.3.3 Results and Discussion

The artificial suction discs with slits and a layer of Ecoflex were capable of adhering to and maintaining grip of rough, granular textures and irregular shapes both underwater and in air. The discs outperformed the commercial suction cup in all experiments except under smooth planar and smooth convex conditions. The most successful prototype iteration was the circular body geometry with four radially symmetric slits and a layer of Ecoflex.

The effects of compliance and soft elastomers

Grip onto the experimental surface was maintained by the soft layer of Ecoflex, which acted much like the soft fibrillar extrusions of the clingfish. Suction discs that did not have a layer of Ecoflex, in addition to the commercially available suction cup, failed to adhere to any of the rocky surfaces presented in Figure 3.7. Thus a layer of soft silicone was crucial to the success on the cratered volcanic and rough granite surfaces.



Figure 3.7: **A** An artificial suction disc picks up a cratered stone. **B** An artificial suction disc picks up the concave surface of a fractured granite rock. **C** An artificial suction disc lifts a 625 gram granite rock. All tests were performed and imaged underwater.

The pull tests performed on a flat textured surface demonstrated the need for a layer of Ecoflex in order to seal the suction chamber on granular surfaces. As shown in Figure 3.8, all prototypes with a layer of Ecoflex adhered to the surface with a surface roughness of 269 μm . Conversely, all prototypes without the Ecoflex layer did not adhere to the surface with the roughness of 269 μm .

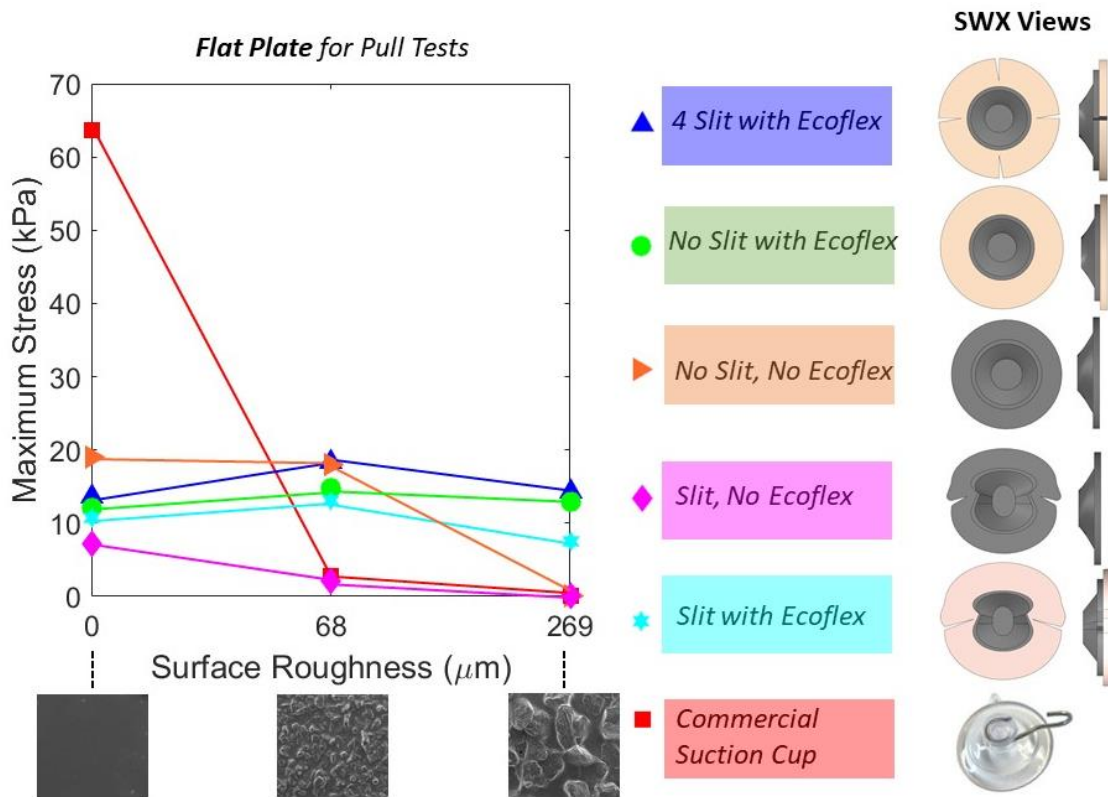


Figure 3.8: Layer of Ecoflex needed for adhesion on rough surfaces, findings of the flat plate pull tests on variable surface roughnesses. Comparison of performance of five prototypes against a commercially available suction cup. Pull test performed in bath of water, three pull tests per disc. “SWX Views” provides ventral and side views of the disc represented in the plot.

None of the prototypes without an Ecoflex layer, with the exception of the circular prototype of only DragonSkin 20, adhered to a flat plate of surface roughness 68 μm . The commercial suction cup, also circular but composed of a stiffer plastic, failed to adhere at this moderate surface roughness of 68 μm . The material stiffness played a key role in the differences of adhesion between the bare circular prototype and the commercial suction cup at the moderate roughness of 68 μm . That is, the DragonSkin20 of the circular prototype was more compliant than the plastic of the commercial suction cup, accounting for greater conformation and sealing of the suction chamber. This compliance yielded a relative success at the moderate surface roughness despite lacking a layer of Ecoflex. In sum, the artificial suction discs outperformed the commercial suction cup on rough surfaces. The performance of the artificial suction discs with Ecoflex performed consistently well across the three tested surface roughnesses.

The maximum stresses of the artificial discs are lower than the maximum stresses recorded by Wainwright et al. 2013. One significant difference between the performance of analog and the biological organism is that not all sections of the disc margin of the analog are in full contact with the substrate. The disc margin of the clingfish, on the other hand, is in full contact during adhesion. This lack of full contact of the artificial suction disc reduces the effective surface area during adhesion. By this reasoning of a reduced effective surface area, the maximum stresses reported in Figure 3.8 may be underestimating the maximum stress that the artificial disc can withstand on rough surfaces.

The artificial discs were tested on convex and concave surfaces. For these pull tests, we selected the best performing prototype, the radially symmetric suction disc with four slits and a 2 mm layer of Ecoflex, and its derivatives to compare its performance against a commercial suction cup.

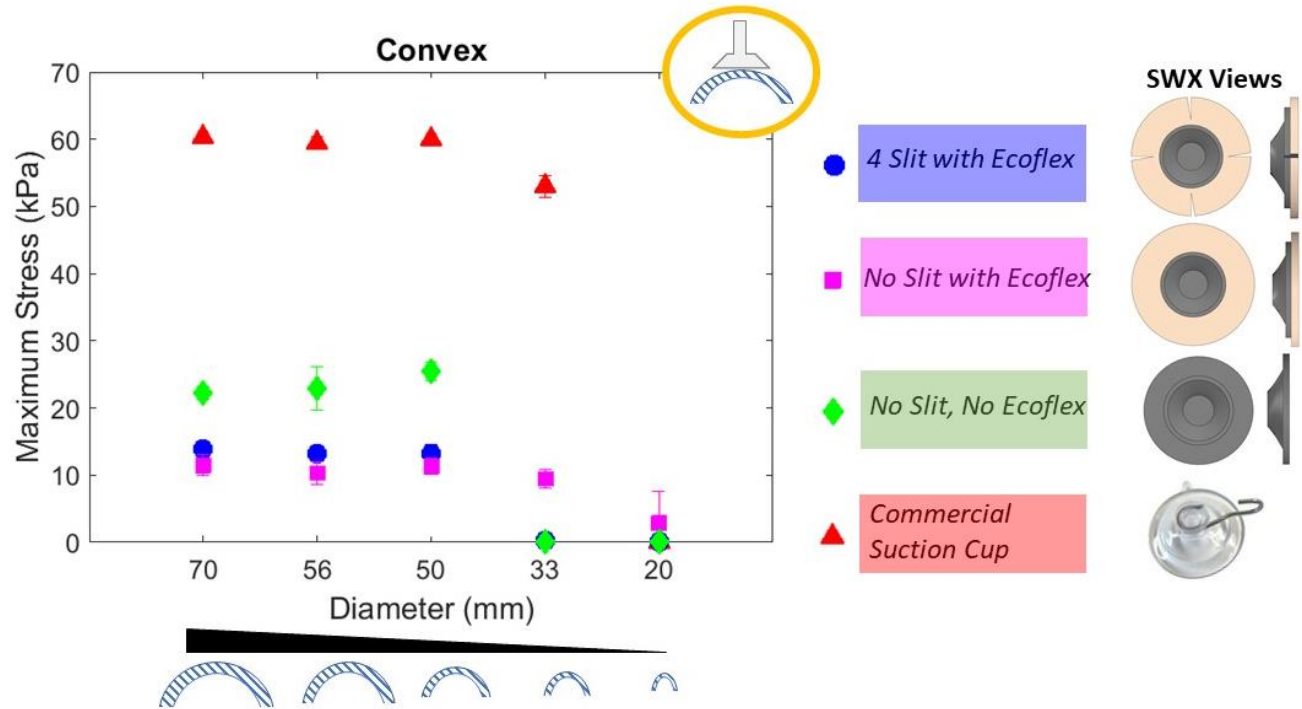


Figure 3.9: Pull-tests on smooth convex surfaces. The commercial suction cup (red triangle) had highest pull-off forces on smooth convex surfaces. Pull test performed in bath of water, three pull tests per disc.

The commercial suction disc performed best across all convex surfaces of decreasing diameter. The artificial suction discs with slits had the lowest performance of the three prototypes on the smooth convex surface of decreasing diameters. The prototype with a layer of Ecoflex and without slits had lower pull-off forces but adhered to smaller diameters in comparison to the bare DragonSkin prototype.

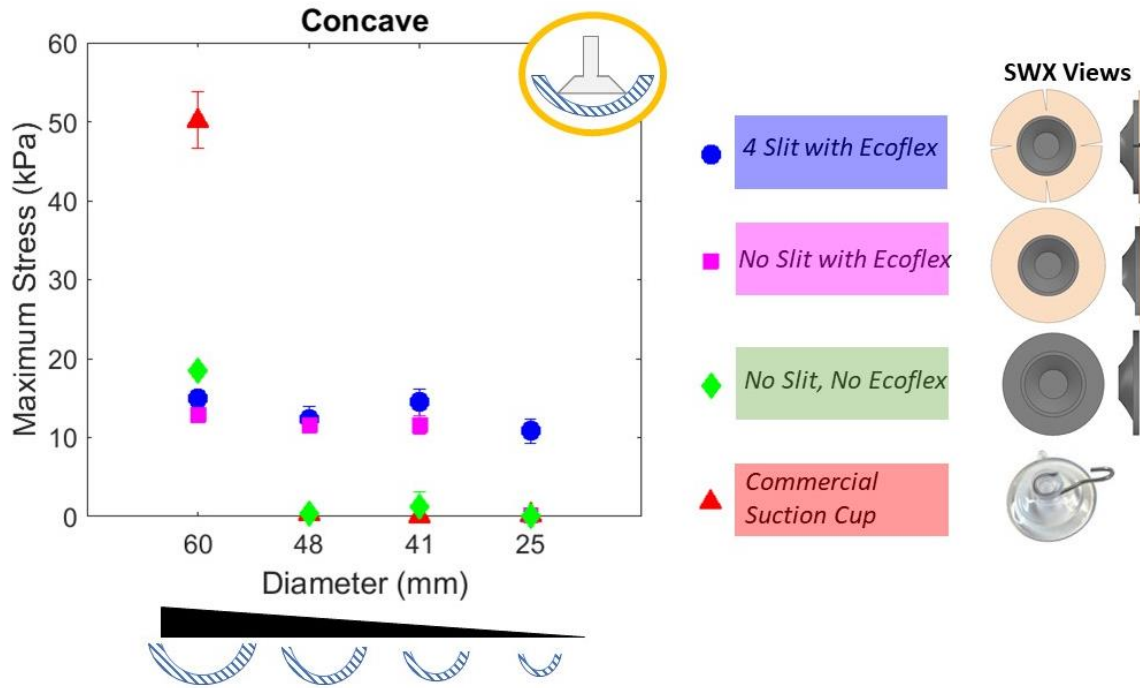


Figure 3.10: Pull-tests on smooth concave surfaces. The artificial disc with a soft layer and four slits had highest adhesive stress at the smallest diameter of a concave surface. Pull-test performed in bath of water, three pull-tests per disc.

The artificial suction disc with four slits and a layer of Ecoflex outperformed the two other artificial suction discs and a commercial suction cup on concave surfaces with small diameters (<48 mm). Only the prototypes with a soft Ecoflex layer were capable of adhering to the smooth concave surfaces that were less than 60 mm diameter. Slits were necessary to achieve adhesion to the smallest diameter of 25 mm. The slits may perhaps allow for a relief in the disc margin, without which may lead to buckling in the silicone. Thus, slits increase adhesion to concave surfaces and decrease adhesion to convex surfaces.

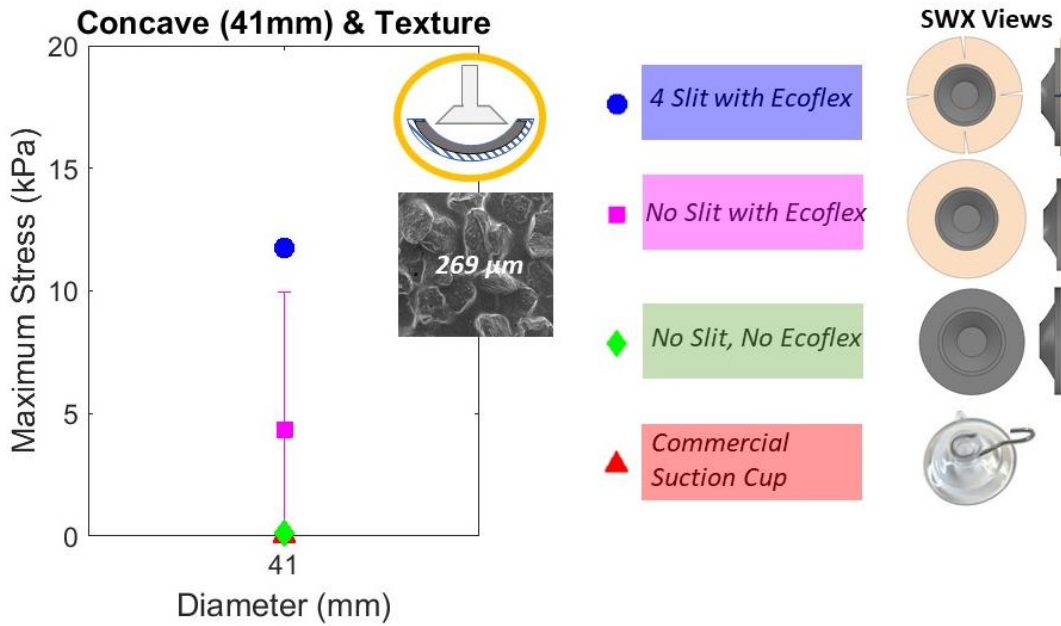


Figure 3.11: Pull-tests on rough concave surface. The discs and commercial suction cups were tested on a concave surface of 41 mm diameter and a roughness of 269 μm . Pull test performed in bath of water, three pull tests per disc.

The artificial suction discs with Ecoflex and slits outperformed all other prototypes and the commercial suction cup for a rough concave surface. The suction disc with Ecoflex and without slits has a significant error bar as it adhered for only one of the three trials.

In sum of the four experimental scenarios, the radially symmetric body geometry was considered optimal for flat surfaces, in comparison to the bilaterally symmetric geometry. This radially symmetric geometry was selected for the trials of concavity. Further, the soft layer of Ecoflex improved performance on rough surfaces. The soft layer acted to increase friction with the rough surfaces, much like the soft fibrils of the clingfish. Slits improved adhesive performance on concave surfaces with small diameters and decreased performance on convex surfaces. Slits provided relief in the disc margin that would have otherwise buckled and

compromised the suction chamber when applied to concave surfaces. The combination of slits and a soft layer was most successful at adhering to rough concave surfaces.

To further our understanding of the effects of slits and a soft layer, the contact area of the suction discs was investigated using Frustrated Total Internal Reflection (FTIR).

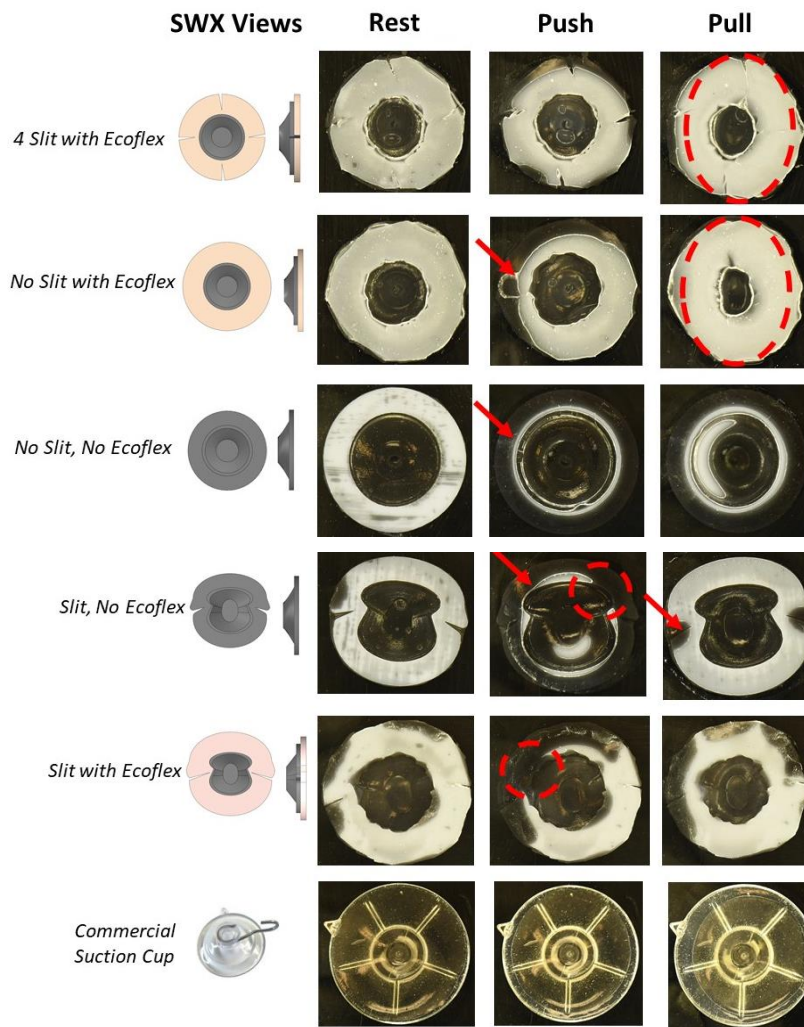


Figure 3.12: Frustrated Total Internal Reflection (FTIR) to visualize the footprint of selected prototypes. The discs were placed on the imaging plate (“Rest”), depressed to the surface (“Push”), and pulled from the surface (“Pull”).

FTIR revealed that the adhesive discs without a soft layer had a significantly smaller effective contact area when pushed to the surface, in comparison to those with a layer of Ecoflex. The greater area of contact of the prototypes with Ecoflex supports the hypothesis that the soft layer increases the frictional footprint, allowing for better adhesion to rough surfaces. The bilaterally symmetric body geometry both with and without a soft layer was unable to seal the suction chamber when depressed to the surface, as indicated by the circled region of Figure 3.12. The layer of Ecoflex on the radially symmetric body geometry increased in eccentricity when pulled, as shown by the dashed ellipse of Figure 3.12. This elongation in the disc margin allowed for deformation of the disc before the seal was compromised. This deformation helps explain the success of the soft layer on concave shapes.

The effects of reliefs in the body cavity

The slits in the body cavity were also critical to successful grip of the artificial discs onto concave surfaces. A slit in the disc margin acted as a relief. Successful adhesion to a non-planar substrate involved maintaining contact with the surface, thereby keeping the low-pressure chamber sealed. In a suction disc without slits, the stiffness of the disc margin limits its performance. The stiffer the material, the harder it becomes to stretch the disc margin over irregular shapes. Disc margins with reliefs were able to stretch more than discs without slits. By allowing more stretch and compliance in the disc margin, the silicone is capable of better conforming to a non-planar shape in order to prevent the loss of vacuum from the low-pressure chamber.

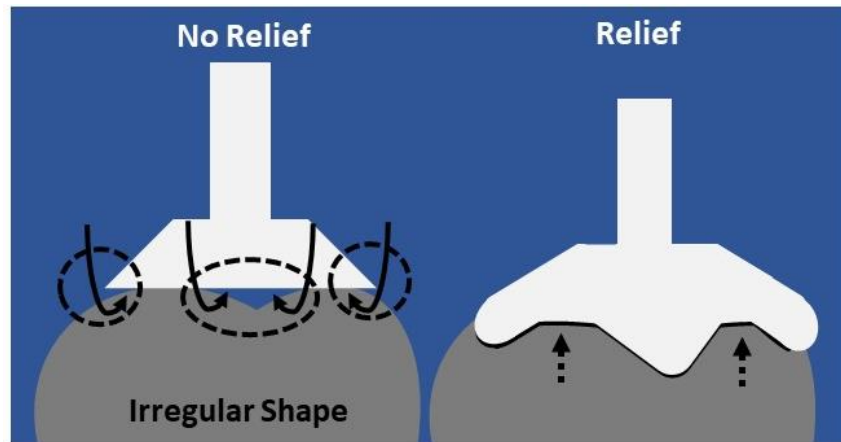


Figure 3.13: Slits are critical to conforming to non-planar shapes of a substrate. **Left** Irregular shapes compromise the low-pressure chamber of suction discs without slits. The disc margin “leaks” without slits. **Right** Slits allow the disc margin to expand and cover irregularities in shape and texture, thus maintaining the seal to the low-pressure chamber.

Amphibious Performance

The artificial discs not only adhere underwater; they also work in air. For instance, as demonstrated in Figure 3.14, a disc was suspended in air and supported a payload that increased in weight. The stone was pressed to the suspended disc to initiate suction. No forms of active suction were used in this experiment to maintain the payload. The adhesion in air and resistance to increasing payloads are promising in consideration of amphibious applications of the clingfish-inspired discs. The commercial suction cup, when subjected to this experiment, failed to adhere onto the river stone, thereby dropping the payload.

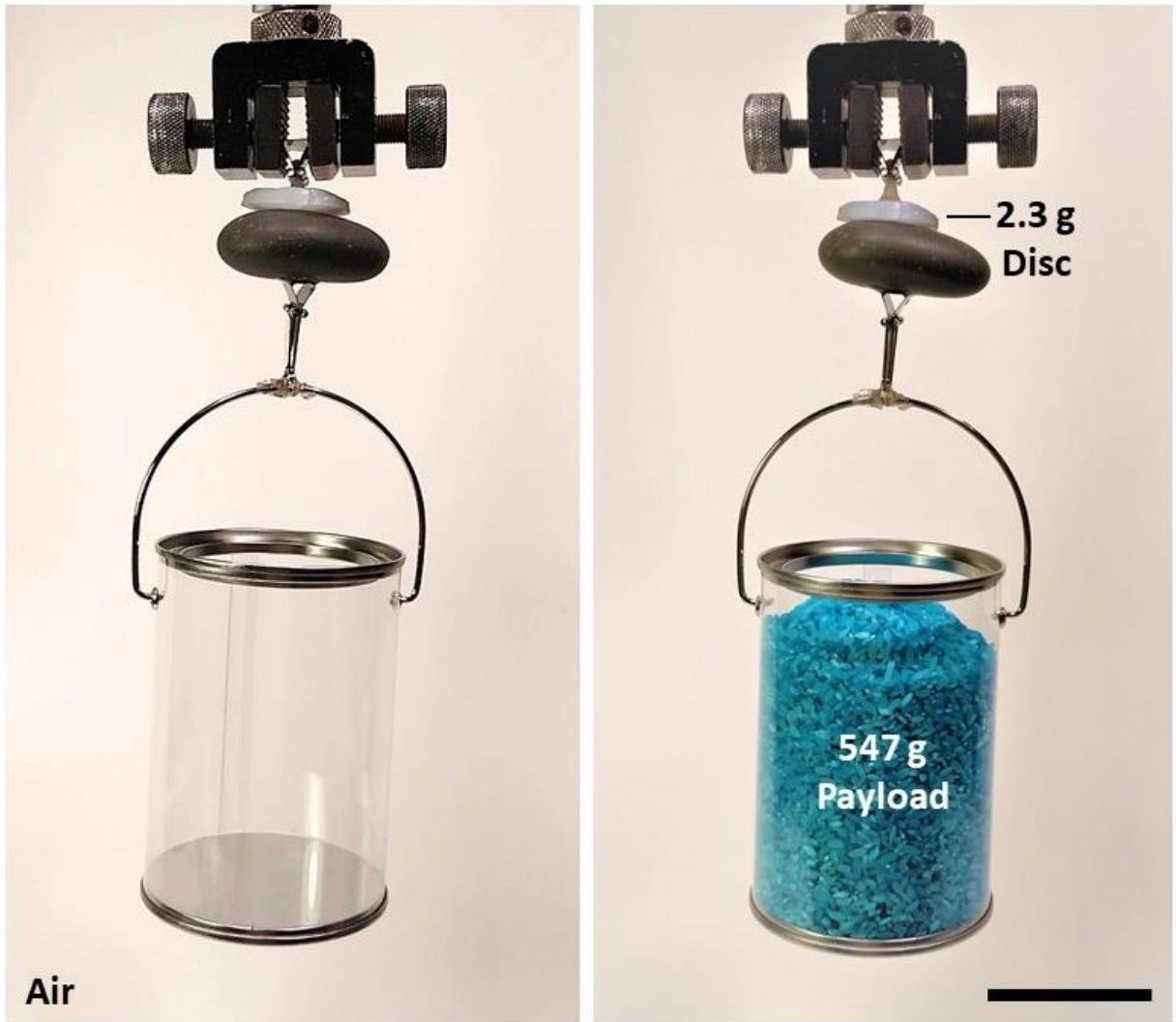


Figure 3.14: A suction disc adheres to a river stone to which a payload is secured and increases in weight overtime. Payload (rice dyed blue for visualization). Performed in air.

3.4 Conclusion and Future Work

The artificial discs outperformed the commercial suction cups on rough surfaces and concave shapes. The discs, weighing 2.3 g, successfully supported loads up to 1.6 pounds in air and underwater. The amphibious nature of the disc may lead to both terrestrial and marine applications of the artificial disc.

In future iterations, mimicking the microscopic sealing fibrils should be explored. As a first step, we have shown that sealing the low-pressure chamber greatly enhances adhesion onto rough surfaces. However, mimicking the microscale features of the fibrillar extrusions may lead to even greater sealing and suction capabilities. We have taken steps towards this research objective, using square silicone micropillars. However, when imaged under FTIR, the micropillars further decreased surface area contact and caused faster disassociation from a surface. By fine-tuning the micropillar structures, it may enhance adhesion.

Future iterations should also begin to incorporate active suction into the disc design. By inducing a vacuum using a pump, greater adhesive strengths are most likely to be achieved and could lead to other provocative applications in robotics.

In sum, this chapter presented a key preliminary step toward achieving reversible adhesion onto variable, non-flat underwater surfaces and will provide a platform which can be applied more generally to robotics in the future. The success of the artificial discs also demonstrates the importance of learning from the repositories of designs provided by natural evolution to improve our current technologies.

Chapter 3, in part is currently being prepared for submission for publication of the material. Sandoval, Jessica; Quan, Haocheng; Deheyn, Dimitri D.; Tolley, Michael T. "A biomimetic suction disc: Design and performance of clingfish-inspired adhesive technology on irregular surfaces". The thesis author was the primary investigator and author of this material.

Chapter 4

Application of the biomimetic suction disc:

Underwater Robotics and Sensing

The artificial suction discs presented in Chapter 3 were successful at creating a seal on highly variable surfaces underwater. This can now be applied to a variety of fields, the three presented in this chapter being archaeology, benthic crawling robots, and sensor platforms. However, this is neither an exhaustive list of applications and can be extended into many other domains, both in dry and aqueous environments.

4.1 Archaeological Applications

Archaeology has been a primary motivator of this project since its infancy. Underwater archaeology requires a soft touch while manipulating artifacts. While this is easily achieved within scuba depths, it become less achievable outside of human diving depths. In order to reach these depths, underwater vehicles, such as Remotely Operated Vehicles (ROVs) and manned

submersibles, perform the majority of deep-sea underwater archaeology. While manipulation is still available to the pilots of these underwater vehicles, a soft touch is much less likely, which increases the risk of damaging the delicate archaeological artifacts. A passive adaptor for the manipulators of underwater vehicles becomes an impactful application of the artificial discs.



Figure 4.1: Suction disc adhering to and lifting an example of an archaeological artifact while underwater.

4.1.1 First iteration of a passive gripper

The first prototypes of a passive underwater gripper involved the use of three suction discs arranged as a tripod. The gripper was a combination of rigid and soft elements, as demonstrated in Figure 4.2. The gripper was printed on the Connex3 Objet350 3D printer as one continuous part. The soft joints were intended to allow for compliance over variable surface topologies.

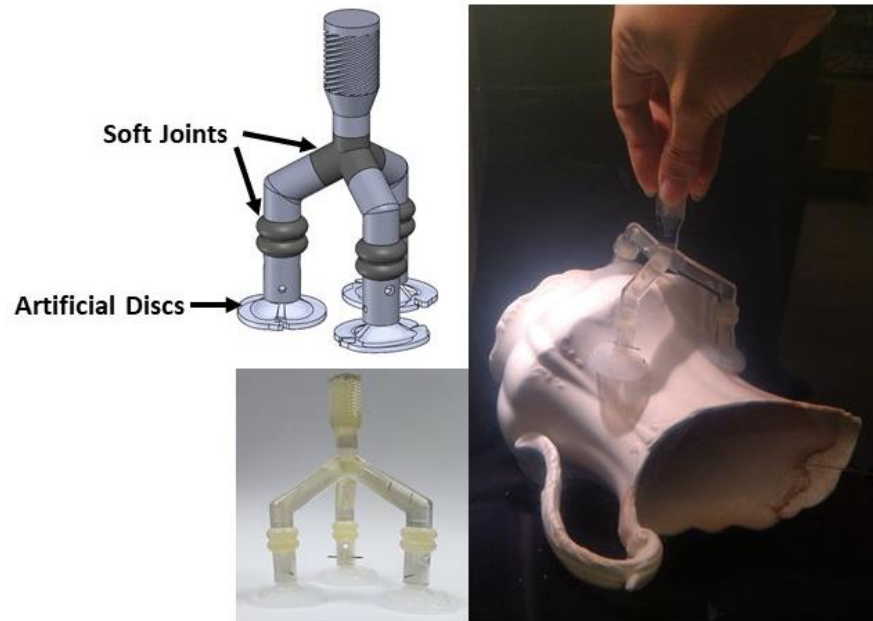


Figure 4.2: The first iteration of the passive gripper was designed for archaeological applications. However, the first iteration was unsuccessful at equally distributing the load across many suction discs.

This first iteration of a passive gripper was unsuccessful at engaging all three suction discs at once. Rather, one suction disc would engage, while the other two were not engaged. As the gripper rotated about the axis of the handle, the suction discs would engage once the surface was roughly perpendicular to the disc margin. Although the substrate was still supported by one disc, the switching of engaged suction discs provided an unreliable gripper. From this prototype, it became clear that the solution to engage all suction discs at once would require a distribution of the load across all discs.

The passive gripper is in the stages of being redesigned with the intention of equally distributing the load across all suction discs for the best grip. By applying the suction discs to manipulators may it help to advance underwater grip in robotics.

4.2 Design of a sensor package

A potential application of the suction discs would be to reversibly adhere sensors onto hard delicate surfaces. One such application is the wildlife monitoring program, CritterCam, which attaches cameras and sensors to animals to understand their behaviors in the wild. These sensor packages are generally secured to organisms using belts and straps to avoid dislodgement and currently includes suction cups for hard shelled organisms. As our experiments have demonstrated, the artificial suction discs outperform commercially available suction cups on rough, irregular surfaces and thus may improve adhesion of sensor packages to hard-shelled organisms.

We developed a camera mount using the clingfish-inspired adhesive technology. An artificial disc, supported by a stiff plastic girdle, balanced an underwater camera on a rough surface. We aim to place these camera mounts onto crustaceans as a preliminary use case.

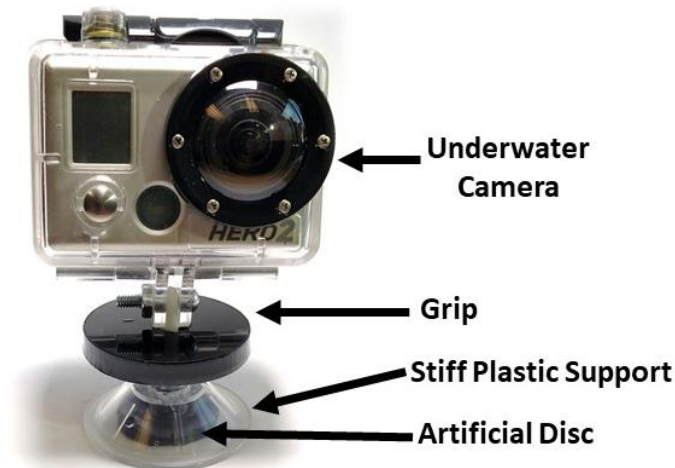


Figure 4.3: Camera mount using an artificial disc to adhere to rough surfaces underwater.

4.3 Application of suction discs to underwater locomotion

Traction is another area that requires reversible directional adhesion to surfaces underwater. The suction discs can be applied to an underwater locomoting robots to improve traction. By doing so, crawling robots can better withstand directional flows while locomoting. The suction discs with a clingfish-inspired geometry would be ideal for this task of underwater traction as the clingfish geometry demonstrated directional adhesion. The circular geometry did not demonstrate directional adhesion. Thus, as legged robot locomotes, a foot strike of the leg engages the suction disc. A forward movement of the leg disengages the suction disc. In order to propel the legged robot forward, the disc must engage and provide traction. The suction discs would thus be able to provide traction and improve locomotion.

4.4 Future applications of the artificial suction disc

The three applications that were discussed in this section are examples of the many fields to which this technology could applied. These fields, although diverse, represent a common need of reliable and reversible underwater grip.

Chapter 4, in part is currently being prepared for submission for publication of the material. Sandoval, Jessica; Quan, Haocheng; Deheyn, Dimitri D.; Tolley, Michael T. "A biomimetic suction disc: Design and performance of clingfish-inspired adhesive technology on irregular surfaces". The thesis author was the primary investigator and author of this material.

Conclusion

The union of the disciplines of engineering and biology fostered the development of an artificial suction disc that mimicked in performance the suction disc of the northern clingfish. We learned from the hierarchical mechanisms of adhesion of the clingfish using electron microscopy and atomic force measurements. The mechanism of adhesion is highly complex in the organism, but can be generalized to a soft compliant suction disc with highly specialized disc margins to allow for sealing on irregular surfaces. The secretions and soft fibrillar extrusions are two of the primary mechanisms in which the low-pressure chamber is sealed.

The biological mimic was able to replicate the geometries and approximate material properties of the low-pressure chamber to allow for conformation to non-planar surfaces. The artificial analog simplified the contributions of the fibrillar structures to a thick layer of soft Ecoflex silicone to provide sealing of the irregularities of a rough surface. In the end, the artificial analog performed significantly better on rough and concave surfaces in comparison to commercial suction cups. Additionally, the artificial discs can support heavy loads in both air in water. These characteristics make the engineered suction discs ideal for application to

underwater manipulation, locomotion, and sensing platforms. By learning from the evolved mechanisms of the clingfish were we able to get a better grip on reversible underwater adhesion.

Bibliography

- [1] L. Heepe and S. N. Gorb, "Biologically Inspired Mushroom-Shaped Adhesive Microstructures," *Annual Review of Materials Research*, vol. 44, pp. 173-203, 2014.
- [2] Y.-C. Chuang, H.-K. Chang, G.-L. Liu and P.-Y. Chen, "Climbing upstream: Multi-scale structural characterization and underwater adhesion of the Pulin river loach (*Sinogastromyzon puliensis*)," *Journal of the Mechanical Behavior of Biomedical Materials*, vol. 73, pp. 76-85, 2017.
- [3] A. Lin, R. Brunner, P. Chen, F. Talke and M. Meyers, "Underwater adhesion of abalone: The role of van der Waals and capillary forces," *Acta Materialia*, no. 57, pp. 4178-4185, 2009.
- [4] A. B. Kesel, A. Martin and T. Seidl, "Getting a grip on spider attachment: an AFM approach to microstructure adhesion in arthropods," *Smart Materials and Structures*, no. 13, pp. 512-518, 2004.
- [5] W. Sun, P. Neuzil, T. Suryadi Kustandi, S. Oh and S. V. D, "The Nature of the Gecko Lizard Adhesive Force," *Biophysical Journal: Biophysical Letters*, 2005.
- [6] S. C. Fischer, E. Arzt and R. Hensel, "Composite Pillars with a Tunable Interface for Adhesion to Rough Substrates," *Applied Materials and Interfaces*, no. 9, pp. 1036-1044, 2017.

- [7] P. Glick, S. A. Suresh, D. I. Ruffatto, M. Cutkosky, M. T. Tolley and A. Parness, "A Soft Robotic Gripper with Gecko-Inspired Adhesive," *IEEE Robotics and Automation Letters*, vol. 3, no. 2, pp. 903-910, 2018.
- [8] M. Culler, K. A. Ledford and J. H. Nadler, "The Role of Topology and Tissue Mechanics in Remora Attachment," *Materials Research Society Symposium Proceedings*, vol. 1648, 2014.
- [9] Y. Wang, X. Yang, Y. Chen, D. K. Wainwright, C. P. Kenaley, G. Zheyuan, Z. Liu, H. Liu, J. Guan, T. Wang, J. C. Weaver, R. J. Wood and L. Wen, "A biorobotic adhesive disc for underwater hitchhiking inspired by the remora suckerfish," *Science Robotics*, vol. 2, no. 10, 2017.
- [10] F. Tramacere, M. Follador, N. M. Pugno and B. Mazzolai, "Octopus-like suction cups: from natural to artificial solutions," *Bioinspiration and Biomimetics*, vol. 10, 2015.
- [11] D. K. Wainwright, T. Kleinteich, A. Kleinteich, S. N. Gorb and S. A. P, "Stick tight: suction adhesion on irregular surfaces in the northern clingfish," *Biology Letters*, no. 9, 2013.
- [12] D. M. Green and L. D. Barber, "The ventral adhesive disc of the clingfish *Gobiesox maeandricus*: integumental structure and adhesive mechanisms," *Canadian Journal of Zoology*, vol. 66, pp. 1610-1619, 1987.

- [13] K. C. Galloway, K. P. Becker, B. Phillips, J. Kirby, S. Licht, D. Tchernov, R. J. Wood and D. F. Gruber, "Soft Robotic Grippers for Biological Sampling on Deep Reefs," *Soft Robotics*, vol. 3, no. 1, pp. 23-33, 2016.
- [14] S. Licht, E. Collins, M. L. Mendes and C. Baxter, "Stronger at depth: Jamming grippers as deep sea sampling tools," *Soft Robotics*, vol. 4, no. 4, pp. 305-316, 2017.
- [15] K. Mizushima, T. Nishimura, Y. Suzuki, T. Tsuji and T. Watanabe, "Surface Texture of Deformable Robotic Fingertips for a Stable Grasp under both Dry and Wet Conditions," *IEEE Robotics and Automation Letters*, 2017.
- [16] D. M. Green and L. D. Barber, "The ventral adhesive disc of the clingfish *Gobiesox maeandricus*: integumental structure and adhesive mechanisms," *Canadian Journal of Zoology*, no. 66, pp. 1610-1619, 1988.
- [17] K. Autumn, Y. A. Liang, T. S. Hsieh, W. Zesch, W. Pang Chan, T. W. Kenny, R. Fearing and R. J. Full, "Adhesive force of a single gecko foot-hair," *Nature*, vol. 405, pp. 681-685, 2000.
- [18] M. A. North, C. A. Del Grosso and J. J. Wilker, "High Strength Underwater Bonding with Polymer Mimics of Mussel Adhesive Proteins," *Applied Materials and Interfaces*, no. 9, pp. 7866-7872, 2017.
- [19] R. Santos, S. Gorb, V. Jamar and P. Flammang, "Adhesion of echinoderm tube feet to rough surfaces," *The Journal of Experimental Biology*, no. 208, pp. 2555-2567, 2005.

- [20] F. A. Guardiola, M. Cuartero, M. d. M. A. M. Collado-González, F. G. Díaz Baños, J. Meseguer, A. Cuesta and M. A. Esteban, "Description and comparative study of physico-chemical parameters of the teleost fish skin mucus," *Biorheology*, no. 52, pp. 247-256, 2015.
- [21] N. Gravish and G. V. Lauder, "Robotics-inspired biology," *Journal of Experimental Biology*, vol. 221, 2018.
- [22] J. Zou, J. Wang and C. Ji, "The Adhesive System and Anisotropic Shear Force of Guizhou Gastromyzontidae," *Scientific Reports*, 2016.
- [23] P. Ditsche, D. K. Wainwright and A. P. Summers, "Attachment to challenging substrates – fouling, roughness and limits of adhesion in the northern clingfish (*Gobiesox maeandricus*)," *The Journal of Experimental Biology*, vol. 217, pp. 2548-2554, 2014.
- [24] T. Kampowski, L. Eberhard, F. Gallenmuller, T. Speck and S. Poppinga, "Functional morphology of suction discs and attachment performance of the Mediterranean medicinal leech (*Hirudo verbana* Carena)," *Journal of The Royal Society Interface*, vol. 13, no. 117.
- [25] A. M. Smith, "The Structure and Function of Adhesive Gels from Invertebrates," *Integrative and Comparative Biology*, no. 42, pp. 1164-1171, 2002.
- [26] C. Franz and P.-H. Puech, "Atomic Force Microscopy: A Versatile Tool for Studying Cell Morphology, Adhesion and Mechanics," *Cellular and Molecular Bioengineering*, vol. 1, no. 4, pp. 289-300, 2008.

- [27] M. Beckert, B. E. Flammang and J. H. Nadler, "A Model of Interfacial Permeability for Soft Seals in Marine-Organism, Suction-Based Adhesion," *MRS Advances*, pp. 1-13, 2016.
- [28] B. Fulcher and P. Motta, "Suction disk performance of echeneid fishes," *Canadian Journal of Zoology*, no. 84, pp. 42-50, 2006.
- [29] J. De Meyer and T. Geerinckx, "Using the Whole Body as a Sucker: Combining Respiration and Feeding with an Attached Lifestyle in Hill Stream Loaches (Balitoridae, Cypriniformes)," *Journal of Morphology*, no. 275, pp. 1066-1079, 2014.
- [30] A. Parness, D. Soto, N. Esparza, N. Gravish, M. Wilkinson, K. Autumn and M. Cutkosky, "A microfabricated wedge-shaped adhesive array displaying gecko-like dynamic adhesion, directionality and long lifetime," *Journal of The Royal Society Interface*, no. 6, pp. 1223-1232, 2009.
- [31] A. Y. Stark, I. Badge, N. A. Wucinich, W. W. Sullivan, P. H. Niewiarowski and A. Dhinojwala, "Surface wettability plays a significant role in gecko adhesion underwater," *PNAS*, vol. 110, no. 16, pp. 6340-6345, 2013.
- [32] A. Sadeghi and L. Beccai, "Design and Development of Innovative Adhesive Suckers Inspired by the Tube Feet of Sea Urchins," *The Fourth IEEE RAS/EMBS International Conference on Biomedical Robotics and Biomechatronics* , pp. 617-622, 2012.
- [33] T. Takahashi, M. Suzuki and S. Aoyagi, "Octopus Bioinspired Vacuum Gripper with Micro Bumps," *Proceedings of the 11th IEEE Annual International Conference on Nano/Micro Engineered and Molecular Systems (NEMS)* , 2016.

[34] T. H. Pires and F. Z. Gibran, "Intertidal life: field observations on the clingfish *Gobiesox barbatulus* in southeastern Brazil," *Neotropical Ichthyology*, vol. 9, no. 1, pp. 233-240, 2011.

[35] J. Y. Han, "Low-cost multi-touch sensing through frustrated total internal reflection," *Proceedings of the 18th annual ACM symposium on User interface software and technology*, pp. 115-118, 2005.